

1 **Where is Late Cenozoic climate change most likely to impact** 2 **denudation?**

3

4 Sebastian G. Mutz¹, Todd A. Ehlers¹, Martin Werner², Gerrit Lohmann², Christian Stepanek²,
5 Jingmin Li^{1,3}

6 ¹Department of Geosciences, University Tübingen, D-72074 Tübingen, Germany

²Department of Paleoclimate Dynamics, Alfred Wegener Institute, Helmholtz Centre for Polar and Marine Research, D-
27570 Bremerhaven, Germany

³now at Institute for Geography and Geology, University of Würzburg, Würzburg, D-97074 Germany

7

8 *Correspondence to:* Sebastian G. Mutz (sebastian.mutz@uni-tuebingen.de)

9

10 **Abstract**

11 The denudation history of active orogens is often interpreted in the context of modern climate and vegetation gradients.
12 Here we address the validity of this approach and ask the question: what are the spatial and temporal variations in
13 palaeoclimate for a latitudinally diverse range of active orogens? We do this using high-resolution (T159, ca. 80 x 80
14 km at the equator) palaeoclimate simulations from the ECHAM5 global Atmospheric General Circulation Model and a
15 statistical cluster analysis of climate over different orogens (Andes, Himalaya, SE Alaska, Pacific NW USA). Time
16 periods and boundary conditions considered include the Pliocene (PLIO, ~3 Ma), the Last Glacial Maximum (LGM,
17 ~21 ka), Mid Holocene (MH, ~6 ka) and Pre-Industrial (PI, reference year 1850). The regional simulated climates of
18 each orogen are described by means of cluster analyses based on the variability of precipitation, 2m air temperature, the
19 intra-annual amplitude of these values, and monsoonal wind speeds where appropriate. Results indicate the largest
20 differences to the PI climate existed for the LGM and PLIO climates in the form of widespread cooling and reduced
21 precipitation in the LGM and warming and enhanced precipitation during the PLIO. The LGM climate shows the
22 largest deviation in annual precipitation from the PI climate, and shows enhanced precipitation in the temperate Andes,
23 and coastal regions for both SE Alaska and the US Pacific Northwest . Furthermore, LGM precipitation is reduced in
24 the western Himalayas and enhanced in the eastern Himalayas, resulting in a shift of the wettest regional climates
25 eastward along the orogen. The cluster-analysis results also suggest more climatic variability across latitudes east of the
26 Andes in the PLIO climate than in other time-slice experiments conducted here. Taken together, these results highlight
27 significant changes in Late Cenozoic regional climatology over the last ~3 Ma. Comparison of simulated climate with
28 proxy-based reconstructions for the MH and LGM reveal satisfactory to good performance of the model in reproducing
29 precipitation changes, although in some cases discrepancies between neighbouring proxy observations highlight
30 contradictions between proxy observations themselves. Finally, we document regions where the largest magnitudes of

31 Late Cenozoic changes in precipitation and temperature occur and offer the highest potential for future observational
32 studies that quantify the impact of climate change on denudation and weathering rates.

33

34 **Keywords:** Cenozoic climate, ECHAM5, Last Glacial Maximum, Mid-Holocene, Pliocene, cluster analysis, Himalaya,
35 Tibet, Andes, Alaska, Cascadia

36

37 **1. Introduction**

38 Interpretation of orogen denudation histories in the context of climate and tectonic interactions is often hampered
39 by a paucity of terrestrial palaeoclimate proxy data needed to reconstruct spatial variations in palaeoclimate. While it is
40 self-evident that palaeoclimate changes could influence palaeodenudation rates, it is not always self-evident what the
41 magnitude of climate change over different geologic time scales is, or what geographic locations offer the greatest
42 potential to investigate palaeoclimate impacts on denudation. Palaeoclimate reconstructions are particularly beneficial
43 when denudation rates are determined using geo- and thermo-chronology techniques that integrate over timescales of
44 10^3 - 10^6 years (e.g. cosmogenic radionuclides or low-temperature thermochronology) [e.g., Kirchner et al., 2001;
45 Schaller et al., 2002; Bookhagen et al., 2005; Moon et al., 2011; Thiede and Ehlers, 2013; Lease and Ehlers, 2013].
46 However, few studies using denudation rate determination methods that integrate over longer timescales have access to
47 information about past climate conditions that could influence these palaeo-denudation rates. Palaeoclimate modelling
48 offers an alternative approach to sparsely available proxy data for understanding the spatial and temporal variations in
49 precipitation and temperature in response to changes in orography [e.g. Takahashi and Battisti, 2007a, b; Insel et al.,
50 2010; Feng et al., 2013] and global climate change events [e.g. Salzmann, 2011; Jeffery et al., 2013]. In this study, we
51 characterise the climate at different times in the Late Cenozoic, and the magnitude of climate change for a range of
52 active orogens. Our emphasis is on identifying changes in climate parameters relevant to weathering and catchment
53 denudation to illustrate the potential importance of various global climate change events on surface processes.

54 Previous studies of orogen-scale climate change provide insight into how different tectonic or global climate
55 change events influence regional climate change. For example, sensitivity experiments demonstrated significant
56 changes in regional and global climate in response to landmass distribution and topography of the Andes, including
57 changes in moisture transport, the north-south asymmetry of the Intertropical Convergence Zone [e.g. Takahashi and
58 Battisti, 2007a, ; Insel et al., 2010] and (tropical) precipitation [Maroon et al., 2015, ; 2016]. Another example is the
59 regional and global climate changes induced by the Tibetan Plateau surface uplift due to its role as a physical obstacle
60 to circulation [Raymo and Ruddiman, 1992; Kutzbach et al., 1993; Thomas, 1997; Böhner, 2006; Molnar et al., 2010;
61 Boos and Kuang, 2010]. The role of tectonic uplift in long term regional and global climate change remains a focus of

62 research and continues to be assessed with geologic datasets [e.g. Dettman et al., 2003; Caves et al., 2017; Kent-
63 Corson et al., 2006; Lechler et al., 2013; Lechler and Niemi, 2011; Licht et al., 2016; Methner et al.,
64 2016; Mulch et al., 2015, 2008; Pingel et al., 2016] and climate modelling [e.g. Kutzbach et al., 1989; Kutzbach
65 et al., 1993; Zhisheng, 2001; Böhner, 2006; Takahashi and Battisti, 2007a; Ehlers and Poulsen, 2009; Insel et al., 2010;
66 Boos and Kuang, 2010]. Conversely, climate influences tectonic processes through erosion [e.g. Molnar and England,
67 1990; Whipple et al., 1999; Montgomery et al., 2001; Willett et al., 2006; Whipple, 2009]. Quaternary climate change
68 between glacial and interglacial conditions [e.g. Braconnot et al., 2007; Harrison et al., 2013] resulted in not only the
69 growth and decay of glaciers and glacial erosion [e.g. Yanites and Ehlers, 2012; Herman et al., 2013; Valla et al., 2011]
70 but also global changes in precipitation and temperature [e.g. Otto-Bliesner et al., 2006; Li et al., 2017] that could
71 influence catchment denudation in non-glaciated environments [e.g. Schaller and Ehlers, 2006; Glotzbach et al., 2013;
72 Marshall et al., 2015]. These dynamics highlight the importance of investigating how much climate has changed over
73 orogens that are the focus of studies of climate-tectonic interactions and their impact on erosion.

74 Despite recognition by previous studies that climate change events relevant to orogen denudation are prevalent
75 throughout the Late Cenozoic, few studies have critically evaluated how different climate change events may, or may
76 not, have affected the orogen climatology, weathering and erosion. Furthermore, recent controversy exists concerning
77 the spatial and temporal scales over which geologic and geochemical observations can record climate-driven changes in
78 weathering and erosion [e.g. Whipple, 2009; von Blanckenburg et al., 2015; Braun, 2016]. For example, the previous
79 studies highlight that although palaeoclimate impacts on denudation rates are evident in some regions and measurable
80 with some approaches, they are not always present (or detectable) and the spatial and temporal scale of climate change
81 influences our ability to record climate sensitive denudation histories. This study contributes to our understanding of
82 the interactions between climate, weathering, and erosion by bridging the gap between the palaeoclimatology and
83 surface processes communities by documenting the magnitude and distribution of climate change over tectonically
84 active orogens.

85 In this study, we employ the ECHAM5 global Atmospheric General Circulation Model and document climate
86 and climate change for time slices ranging between the Pliocene (PLIO, ~3 Ma) to pre-industrial (PI) times for the St.
87 Elias Range of South East Alaska, the US Pacific Northwest (Olympic and Cascade Range), western South America
88 (Andes) and South Asia (incl. parts of Central- and East Asia). Our approach is two-fold and includes:

89 1. An empirical characterisation of palaeo-climates in these regions based on the covariance and spatial
90 clustering of monthly precipitation and temperature, the monthly change in precipitation and temperature magnitude,
91 and wind speeds where appropriate.

92 2. Identification of changes in annual mean precipitation and temperature in selected regions for four time
93 periods: (PLIO, Last Glacial Maximum (LGM), the Mid-Holocene (MH) and PI) and subsequent validation of the

94 simulated precipitation changes for MH and LGM.
95 Our focus is on documenting climate and climate change in different locations with the intent of informing past and
96 ongoing palaeodenudation studies of these regions. The results presented here also provide a means for future work to
97 formulate testable hypotheses and investigations into whether or not regions of large palaeoclimate change produced a
98 measurable signal in denudation rates. In this study, we intentionally refrain from applying predicted palaeoclimate
99 changes to predict denudation rate changes. Such a prediction is beyond the scope of this study because a convincing
100 (and meaningful) calculation of climate-driven transients in fluvial erosion (e.g. via the kinematic wave equation),
101 variations in frost cracking intensity, or changes in hillslope sediment production and transport at the large regional
102 scales considered here is not tractable within a single manuscript, and instead is the focus of our ongoing work. Instead,
103 our emphasis lies on addressing the first question we are confronted with in our own research into denudation rate
104 studies around world, namely - where is Late Cenozoic climate change most likely to impact denudation?

105

106 **2. Methods: Climate modelling and cluster analyses for climate characterisation**

107

108 **2.1 ECHAM5 simulations**

109 The global Atmospheric General Circulation Model ECHAM5 [Roeckner et al., 2003] has been developed at the
110 Max Planck Institute for Meteorology and is based on the spectral weather forecast model of the ECMWF [Simmons et
111 al., 1989]. In the context of palaeoclimate applications, the model has been used mostly at lower resolution (T31, ca.
112 $3.75^{\circ} \times 3.75^{\circ}$; T63, ca. $1.9^{\circ} \times 1.9^{\circ}$ in case of Feng et al. [2016] and T106 in the case of Li et al. [2016] and Feng and
113 Poulsen [2016]). The performed studies are not limited to the last millenium [e.g. Jungclaus et al., 2010] but also
114 include research in the field of both warmer and colder climates, at orbital [e.g. Gong et al., 2013; Lohmann et al., 2013;
115 Pfeiffer and Lohmann, 2016; Zhang et al., 2013a; Zhang et al., 2014; Wei and Lohmann, 2012] and tectonic time scales
116 [e.g. Knorr et al., 2011; Stepanek and Lohmann, 2012], and under anthropogenic influence [Gierz et al., 2015].

117 Here, the ECHAM5 simulations were conducted at a T159 spatial resolution (horizontal grid size ca. 80 km x 80
118 km at the equator) with 31 vertical levels (between the surface and 10hPa). This high model resolution is admittedly not
119 required for all of the climatological questions investigated in this study, and it should be noted that the skill of GCM's
120 in predicting orographic precipitation remains limited at this scale [e.g. Meehl et al. 2007]. However, simulations were
121 conducted at this resolution so that future work can apply the results in combination with different dynamical and
122 statistical downscaling methods to quantify changes at large catchment to orogen scales. The output frequency is
123 relatively high (1 day) to enhance the usefulness of our simulations as input for landscape evolution and other models
124 that may benefit from daily input. The simulations were conducted for five different time periods: present-day (PD), PI,
125 MH, LGM and PLIO.

126 A PD simulation (not shown here) was used to establish confidence in the model performance before conducting
127 palaeosimulations and has been compared with the following observation-based datasets: European Centre for Medium-
128 Range Weather Forecasts (ECMWF) re-analyses [ERA40, Uppala et al., 2005], National Centers for Environmental
129 Prediction and National Center for Atmospheric Research (NCEP/NCAR) re-analyses [Kalnay et al., 1996; Kistler et
130 al., 2001], NCEP Regional Reanalysis (NARR) [Mesinger et al., 2006], the Climate Research Unit (CRU) TS3.21
131 dataset [Harris et al., 2013], High Asia Refined Analysis (HAR30) [Maussion et al., 2014] and the University of
132 Delaware dataset (UDEL v3.01) [Legates et al., 1990]. (See Mutz et al. [2016] for a detailed comparison with a lower
133 resolution model).

134 The PI climate simulation is an ECHAM5 experiment with PI (reference year 1850) boundary conditions. Sea
135 Surface Temperatures (SST) and Sea Ice Concentration (SIC) are derived from transient coupled ocean-atmosphere
136 simulations [Lorenz and Lohmann, 2004; Dietrich et al., 2013]. Following Dietrich et al. [2013], greenhouse gas
137 (GHG) concentrations (CO₂: 280 ppm) are taken from ice core based reconstructions of CO₂ [Etheridge et al., 1996],
138 CH₄ [Etheridge et al., 1998] and N₂O [Sowers et al., 2003]. Sea surface boundary conditions for MH originate from a
139 transient, low-resolution, coupled atmosphere-ocean simulation of the mid (6 ka) Holocene [Wei and Lohmann, 2012;
140 Lohmann et al., 2013], where the GHG concentrations (CO₂: 280 ppm) are taken from ice core reconstructions of
141 GHG's by Etheridge et al. [1996], Etheridge et al. [1998] and Sowers et al. [2003]. GHG's concentrations for the LGM
142 (CO₂: 185 ppm) have been prescribed following Otto-Bliesner et al. [2006]. Orbital parameters for MH and LGM are
143 set according to Dietrich et al. [2013] and Otto-Bliesner et al. [2006], respectively. LGM land-sea distribution and ice
144 sheet extent and thickness are set based on the PMIP III (Palaeoclimate Modelling Intercomparison Project, phase 3)
145 guidelines (elaborated on by Abe-Ouchi et al [2015]). Following Schäfer-Neth and Paul [2003], SST and SIC for the
146 LGM are based on GLAMAP [Sarnthein et al. 2003] and CLIMAP [CLIMAP project members, 1981] reconstructions
147 for the Atlantic and Pacific/Indian Ocean, respectively. Global MH and LGM vegetation are based on maps of plant
148 functional types by the BIOME 6000 / Palaeovegetation Mapping Project [Prentice et al., 2000; Harrison et al., 2001;
149 Bigelow et al., 2003; Pickett et al., 2004] and model predictions by Arnold et al. [2009]. Boundary conditions for the
150 PLIO simulation, including GHG concentrations (CO₂: 405), orbital parameters and surface conditions (SST, SIC, sea
151 land mask, topography and ice cover) are taken from the PRISM (Pliocene Research, Interpretation and Synoptic
152 Mapping) project [Haywood et al., 2010; Sohl et al., 2009; Dowsett et al., 2010], specifically PRISM3D. The PLIO
153 vegetation boundary condition was created by converting the PRISM vegetation reconstruction to the JSBACH plant
154 functional types as described by Stepanek and Lohmann [2012], but the built-in land surface scheme was used

155 SST reconstructions can be used as an interface between oceans and atmosphere [e.g. Li et al. 2016] instead of
156 conducting the computationally more expensive fully coupled Atmosphere-Ocean GCM experiments. While the use of
157 SST climatologies comes at the cost of capturing decadal-scale variability, and the results are ultimately biased towards

158 the SST reconstructions the model is forced with, the simulated climate more quickly reaches an equilibrium state and
159 the means of atmospheric variables used in this study do not change significantly after the relatively short spin-up
160 period. The palaeoclimate simulations (PI, MH, LGM, PLIO) using ECHAM5 are therefore carried out for 17 model
161 years, of which the first two years are used for model spin up. The monthly long-term averages (multi-year means for
162 individual months) for precipitation, temperature, as well as precipitation and temperature amplitude, i.e. the mean
163 difference between the hottest and coldest months, have been calculated from the following 15 model years for the
164 analysis presented below.

165 For further comparison between the simulations, the investigated regions were subdivided (Fig. 1). Western
166 South America was subdivided into four regions: parts of tropical South America (80°-60° W, 23.5°-5° S), temperate
167 South America (80°-60° W, 50°-23.5° S), tropical Andes (80°-60° W, 23.5°-5° S; high-pass filtered), i.e. most of the
168 Peruvian Andes, Bolivian Andes and northernmost Chilean Andes, and temperate Andes (80°-60° W, 50°-23.5° S,
169 high-pass filtered). South Asia was subdivided into three regions: tropical South Asia (40°-120°E, 0°-23.5°N),
170 temperate South Asia (40°-120°E, 23.5°-60°N), and high altitude South Asia (40°-120°E, 0°-60°N; high-pass filtered).

171 Our approach of using a single GCM (ECHAM5) for our analysis is motivated by, and differs from, previous
172 studies where inter-model variability exists from the use of different GCMs due to different parameterisations in each
173 model. The variability in previous inter-model GCM comparisons exists despite the use of the same forcings [e.g. see
174 results highlighted in IPCC AR5]. Similarities identified between these palaeoclimate simulations conducted with
175 different GCMs using similar boundary conditions can establish confidence in the models when in agreement with
176 proxy reconstructions. However, differences identified in inter-model GCM comparisons highlight biases by all or
177 specific GCMs, or reveal sensitivities to one changed parameter, such as model resolution. Given these limitations of
178 GCM modelling, we present in this study a comparison of a suite of ECHAM5 simulations to proxy-based
179 reconstructions (where possible) and, to a lesser degree, comment on general agreement or disagreement of our
180 ECHAM5 results with other modelling studies. A detailed inter-model comparison of our results with other GCMs is
181 beyond the scope of this study, and better suited for a different study in a journal with a different focus and audience.
182 Rather, by using the same GCM and identical resolution for the time slice experiments, we reduce the number of
183 parameters (or model parameterisations) varying between simulations and thereby remove potential sources of error or
184 uncertainty that would otherwise have to be considered when comparing output from different models with different
185 parameterisations of processes, model resolution, and in some cases model forcings (boundary conditions).
186 Nevertheless, the reader is advised to use these model results with the GCM's shortcomings and uncertainties in
187 boundary condition reconstructions in mind. For example, precipitation results may require dynamical or statistical
188 downscaling to increase accuracy where higher resolution precipitation fields are required. Furthermore, readers are
189 advised to familiarise themselves with the palaeogeography reconstruction initiatives and associated uncertainties. For

190 example, while Pliocene ice sheet volume can be estimated, big uncertainties pertaining to their locations remain
191 [Haywood et al. 2010].

192

193 **2.2 Cluster analysis to document temporal and spatial changes in climatology**

194 The aim of the clustering approach is to group climate model surface grid boxes together based on similarities in
195 climate. Cluster analyses are statistical tools that allow elements (i) to be grouped by similarities in the elements'
196 attributes. In this study, those elements are spatial units, the elements' attributes are values from different climatic
197 variables, and the measure of similarity is given by a statistical distance. The four basic variables used as climatic
198 attributes of these spatial elements are: near-surface (2m) air temperature, seasonal 2m air temperature amplitude,
199 precipitation rate, and seasonal precipitation rate amplitude. Since monsoonal winds are a dominant feature of the
200 climate in the South Asia region, near surface (10m) speeds of u-wind and v-wind (zonal and meridional wind
201 components, respectively) during the monsoon season (July) and outside the monsoon season (January) are included as
202 additional variables in our analysis of that region. Similarly, u-wind and v-wind speeds during (January) and outside
203 (July) the monsoon season in South America are added to the list of considered variables to take into account the South
204 American Monsoon System (SASM) in the cluster analysis for this region. The long-term monthly means of those
205 variables are used in a hierarchical clustering method, followed by a non-hierarchical k-means correction with
206 randomised re-groupment [Mutz et al., 2016; Wilks, 2011; Paeth, 2004; Bahrenberg et al., 1992].

207 The hierarchical part of the clustering procedure starts with as many clusters as there are elements (n_i), then
208 iteratively combines the most similar clusters to form a new cluster using centroids for the linkage procedure for
209 clusters containing multiple elements. The procedure is continued until the desired number of clusters (k) is reached.
210 One disadvantage of a pure hierarchical approach is that elements cannot be re-categorised once they are assigned to a
211 cluster, even though the addition of new elements to existing clusters changes the clusters' defining attributes and could
212 warrant a re-categorisation of elements. We address this problem by implementation of a (non-hierarchical) k-means
213 clustering correction [e.g. Paeth, 2004]. Elements are re-categorised based on the multivariate centroids determined by
214 the hierarchical cluster analysis in order to minimize the sum of deviations from the cluster centroids. The
215 Mahalanobis distance [e.g. Wilks, 2011] is used as a measure of similarity or distance between the cluster centroids,
216 since it is a statistical distance and thus not sensitive to different variable units. The Mahalanobis distance also accounts
217 for possible multi-collinearity between variables.

218 The end results of the cluster analyses are subdivisions of the climate in the investigated regions into k
219 subdomains or clusters based on multiple climate variables. The region-specific k has to be prescribed before the
220 analyses. A large k may result in redundant additional clusters describing very similar climates, thereby defeating the
221 purpose of the analysis to identify and describe the dominant, distinctly different climates in the region and their

222 geographical coverage. Since it is not possible to know a priori the ideal number of clusters, k was varied between 3 and
223 10 for each region and the results presented below identify the optimal number of visibly distinctly different clusters
224 from the analysis. Optimal k was determined by assessing the distinctiveness and similarities between the climate
225 clusters in the systematic process of increasing k from 3 to 10. Once an increase in k no longer resulted in the addition
226 of another cluster that was climatologically distinctly different from the others, and instead resulted in at least two
227 similar clusters, k of the previous iteration was chosen as the optimal k for the region.

228 The cluster analysis ultimately results in a description of the geographical extent of a climate (cluster)
229 characterised by a certain combination of mean values for each of the variables associated with the climate. For
230 example, climate cluster 1 may be the most tropical climate in a region and thus be characterised by a high precipitation
231 values, high temperature values and low seasonal temperature amplitude. Each of the results (consisting of the
232 geographical extent of climates and mean vectors describing the climate) can be viewed as an optimal classification for
233 the specific region and time. It serves primarily as a means for providing an overview of the climate in each of the
234 regions at different times, reduces dimensionality of the raw simulation output, and identify regions of climatic
235 homogeneity that is difficult to notice by viewing simple maps of each climate variable. Its synoptic purpose is similar
236 to that of the widely known Köppen-Geiger classification scheme [Peel et al., 2007], but we allow for optimal
237 classification rather than prescribe classes, and our selection of variables is more restricted and made in accordance with
238 the focus of this study.

239

240 **3. Results**

241 Results from our analysis are first presented for general changes in global temperature and precipitation for the
242 different time slices (Fig. 2, 3), which is then followed by an analysis of changes in the climatology of selected orogens.
243 A more detailed description of temperature and precipitation changes in our selected orogens is presented in subsequent
244 subsections (Fig. 4 and following). All differences in climatology are expressed relative to the PI control run. Changes
245 relative to the PI rather than PD conditions are presented to avoid interpreting an anthropogenic bias in the results and
246 focusing instead on pre-anthropogenic variations in climate. For brevity, near-surface (2m) air temperature and total
247 precipitation rate are referred to as temperature and precipitation.

248

249 **3.1 Global differences in mean annual temperature**

250 This section describes the differences between simulated MH, LGM, and PLIO annual mean temperature anom-
251 alies with respect to PI shown in Fig. 2b, and PI temperature absolute values shown in Fig. 2a. Most temperature differ-
252 ences between the PI and MH climate are within -1°C to 1°C . Exceptions to this are the Hudson Bay, Weddell Sea and
253 Ross Sea regions which experience warming of $1-3^{\circ}\text{C}$, $1-5^{\circ}\text{C}$ and $1-9^{\circ}\text{C}$ respectively. Continental warming is mostly

254 restricted to low-altitude South America, Finland, western Russia, the Arabian Peninsula (1-3°C) and subtropical north
255 Africa (1-5°C). Simulation results show that LGM and PLIO annual mean temperature deviate from the PI means the
256 most. The global PLIO warming and LGM cooling trends are mostly uniform in direction, but the magnitude varies re-
257 gionally. The strongest LGM cooling is concentrated in regions where the greatest change in ice extent occurs (as indic-
258 ated on Fig. 2), i.e. Canada, Greenland, the North Atlantic, Northern Europe and Antarctica. Central Alaska shows no
259 temperature changes, whereas coastal South Alaska experiences cooling of $\leq 9^\circ\text{C}$. Cooling in the US Pacific northwest
260 is uniform and between 11 and 13°C. Most of high-altitude South America experiences mild cooling of 1-3°C, 3-5°C in
261 the central Andes and $\leq 9^\circ\text{C}$ in the south. Along the Himalayan orogen, LGM temperature values are 5-7°C below PI
262 values. Much of central Asia and the Tibetan plateau cools by 3-5°C, and most of India, low-altitude China and south-
263 east Asia by 1-3°C.

264 In the PLIO climate, parts of Antarctica, Greenland and the Greenland Sea experience the greatest temperature
265 increase ($\leq 19^\circ\text{C}$). Most of southern Alaska warms by 1-5°C and $\leq 9^\circ\text{C}$ near McCarthy, Alaska. The US Pacific northw-
266 est warms by 1-5°C. The strongest warming in South America is concentrated at the Pacific west coast and the Andes
267 (1-9°C), specifically between Lima and Chiclayo, and along the Chilean-Argentinian Andes south of Bolivia ($\leq 9^\circ\text{C}$).
268 Parts of low-altitude South America to the immediate east of the Andes experience cooling of 1-5°C. The Himalayan
269 orogen warms by 3-9°C, whereas Myanmar, Bangladesh, Nepal, northern India and northeast Pakistan cool by 1-9°C.
270

271 3.2 Global differences in mean annual precipitation

272 Notable differences occur between simulated MH, LGM, PLIO annual mean precipitation anomalies with re-
273 spect to PI shown in Fig. 3b, and the PI precipitation absolute values shown in Fig. 3a. Of these, MH precipitation devi-
274 ates the least from PI values. The differences between MH and PI precipitation on land appear to be largest in northern
275 tropical Africa (increase ≤ 1200 mm/a) and along the Himalayan orogen (increase ≤ 2000 mm/a) and in central Indian
276 states (decrease) ≤ 500 mm. The biggest differences in western South America are precipitation increases in central Chile
277 between Santiago and Puerto Montt. The LGM climate shows the largest deviation in annual precipitation from the PI
278 climate, and precipitation on land mostly decreases. Exceptions are increases in precipitation rates in North American
279 coastal regions, especially in coastal South Alaska (≤ 2300 mm/a) and the US Pacific Northwest (≤ 1700 mm/a). Further
280 exceptions are precipitation increases in low-altitude regions immediately east of the Peruvian Andes (≤ 1800 mm/a),
281 central Bolivia (≤ 1000 mm/a), most of Chile (≤ 1000 mm/a) and northeast India (≤ 1900 mm/a). Regions of notable pre-
282 cipitation decrease are northern Brazil (≤ 1700 mm/a), southernmost Chile and Argentina (≤ 1900 mm/a), coastal south
283 Peru (≤ 700 mm/a), central India (≤ 2300 mm/a) and Nepal (≤ 1600 mm/a).

284 Most of the precipitation on land in the PLIO climate is higher than those in the PI climate. Precipitation is en-
285 hanced by ca. 100-200 mm/a in most of the Atacama desert, by ≤ 1700 mm/a south of the Himalayan orogen and by

286 ≤ 1400 mm/a in tropical South America. Precipitation significantly decreases in central Peru (≤ 2600 mm), southernmost
287 Chile (≤ 2600 mm) and from eastern Nepal to northernmost northeast India (≤ 2500 mm).

288

289 **3.3 Palaeoclimate characterisation from the cluster analysis and changes in regional climatology**

290 In addition to the above described global changes, the PLIO to PI regional climatology changes substantially in
291 the four investigated regions of: South Asia (section 3.3.1), the Andes (section 3.3.2), South Alaska (section 3.3.3) and
292 the Cascade Range (section 3.3.4). Each climate cluster defines separate distinct climate that is characterized by the
293 mean values of the different climate variables used in the analysis. The clusters are calculated by taking the arithmetic
294 means of all the values (climatic means) calculated for the grid boxes within each region. The regional climates are
295 referred to by their cluster number C_1, C_2, \dots, C_k , where k is the number of clusters specified for the region. The clusters
296 for specific palaeoclimates are mentioned in the text as $C_{i(t)}$, where i corresponds to the cluster number ($i=1, \dots, k$) and t
297 to the simulation time period ($t=PI, MH, LGM, PLIO$). The descriptions first highlight the similarities and then the
298 differences in regional climate. The cluster means of seasonal near-surface temperature amplitude and seasonal
299 precipitation amplitude are referred to as temperature and precipitation amplitude. The median, 25th percentile, 75th
300 percentile, minimum and maximum values for annual mean precipitation are referred to as $P_{md}, P_{25}, P_{75}, P_{min}$ and P_{max}
301 respectively. Likewise, the same statistics for temperature are referred to as $T_{md}, T_{25}, T_{75}, T_{min}$ and T_{max} . These are
302 presented as boxplots of climate variables in different time periods. When the character of a climate cluster is described
303 as “high”, “moderate” and “low”, the climatic attribute’s values are described relative to the value range of the specific
304 region in time, thus high PLIO precipitation rates may be higher than high LGM precipitation rates. The character is
305 presented a raster plots, to allow compact visual representation of it. The actual mean values for each variable in every
306 time-slice and region-specific cluster are included in tables in the supplementary material.

307

308 **3.3.1 Climate change and palaeoclimate characterisation in South Asia, Central- and East Asia**

309 This section describes the regional climatology of the four investigated Cenozoic time slices and how
310 precipitation and temperature changes from PLIO to PI times in tropical, temperate and high altitude regions. LGM and
311 PLIO simulations show the largest simulated temperature and precipitation deviations (Fig. 4b) from PI temperature and
312 precipitation (Fig. 4a) in the South Asia region. LGM temperatures are 1-7°C below PI temperatures and the direction
313 of deviation is uniform across the study region. PLIO temperature is mostly above PI temperatures by 1-7°C. The
314 cooling of 3-5°C in the region immediately south of the Himalayan orogen represents one of the few exceptions.
315 Deviations of MH precipitation from PI precipitation in the region are greatest along the eastern Himalayan orogeny,
316 which experiences an increase in precipitation (≤ 2000 mm/a). The same region experiences a notable decrease in
317 precipitation in the LGM simulation, which is consistent in direction with the prevailing precipitation trend on land

318 during the LGM. PLIO precipitation on land is typically higher than PI precipitation.

319 Annual means of precipitation and temperature spatially averaged for the regional subdivisions and the different
320 time slice simulations have been compared. The value range P_{25} to P_{75} of precipitation is higher for tropical South Asia
321 than for temperate and high altitude South Asia (Fig. 5 a-c). The LGM values for P_{25} , P_{md} and P_{75} are lower than for the
322 other time slice simulations, most visibly for tropical South Asia (ca. 100 mm/a). The temperature range (both $T_{75}-T_{25}$
323 and $T_{max}-T_{min}$) is smallest in the hot (ca. 21°C) tropical South Asia, wider in the high altitude (ca. -8°C) South Asia, and
324 widest in the temperate (ca. 2°C) South Asia region (Fig. 5 d-f). T_{md} , T_{25} and T_{75} values for the LGM are ca. 1°C, 1-2°C
325 and 2°C below PI and MH temperatures in tropical, temperate and high altitude South Asia respectively, whereas the
326 same temperature statistics for the PLIO simulation are ca. 1°C above PI and MH values in all regional subdivisions
327 (Fig. 5 d-f). With respect to PI and MH values, precipitation and temperature are generally lower in the LGM and
328 higher in the PLIO in tropical, temperate and high altitude South Asia.

329 In all time periods, the wettest climate cluster C_1 covers an area along the southeastern Himalayan orogen (Fig. 6
330 a-d) and is defined by the highest precipitation amplitude (dark blue, Fig. 6 e-h). $C_{5(PI)}$, $C_{3(MH)}$, $C_{4(LGM)}$ and $C_{5(PLIO)}$ are
331 characterized by (dark blue, Fig. 6e-h) the highest temperatures, u-wind and v-wind speeds during the summer monsoon
332 in their respective time periods, whereas $C_{4(PI)}$, $C_{5(MH)}$, and $C_{6(LGM)}$ are defined by low temperatures and highest
333 temperature amplitude, u-wind and v-wind speeds outside the monsoon season (in January) in their respective time
334 periods (Fig. 6 e-h). The latter 3 climate classes cover much of the more continental, northern landmass in their
335 respective time periods and represents a cooler climate affected more by seasonal temperature fluctuations (Fig. 6 a-d).
336 The two wettest climate clusters C_1 and C_2 are more restricted to the eastern end of the Himalayan orogen in the LGM
337 than during other times, indicating that the LGM precipitation distribution over the South Asia landmass is more
338 concentrated in this region than in other time slice experiments.

339 340 **3.3.2 Climate change and palaeoclimate characterisation in the Andes, Western South America**

341 This section describes the cluster analysis based regional climatology of the four investigated Late Cenozoic
342 time slices and illustrates how precipitation and temperature changes from PLIO to PI in tropical and temperate low-
343 and high altitude (i.e. Andes) regions in western South America (Fig. 7-9).

344 LGM and PLIO simulations show the largest simulated deviations (Fig. 7b) from PI temperature and
345 precipitation (Fig. 7a) in western South America. The direction of LGM temperature deviations from PI temperatures is
346 negative and uniform across the region. LGM temperatures are typically 1-3°C below PI temperatures across the region,
347 and 1-7°C below PI values in the Peruvian Andes, which also experience the strongest and most widespread increase in
348 precipitation during the LGM (≤ 1800 mm/a). Other regions, such as much of the northern Andes and tropical South
349 America, experience a decrease of precipitation in the same experiment. PLIO temperature is mostly elevated above PI

350 temperatures by 1-5°C. The Peruvian Andes experience a decrease in precipitation ($\leq 2600\text{mm}$), while the northern
351 Andes are wetter in the PLIO simulation compared to the PI control simulation.

352 PI, MH, LGM and PLIO precipitation and temperature means for regional subdivisions have been compared.
353 The P_{25} to P_{75} range is smallest for the relatively dry temperate Andes and largest for tropical South America and the
354 tropical Andes (Fig. 8 a-d). P_{max} is lowest in the PLIO in all four regional subdivisions even though P_{md} , P_{25} and P_{75} in
355 the PLIO simulation are similar to the same statistics calculated for PI and MH time slices. P_{md} , P_{25} and P_{75} for the LGM
356 are ca. 50 mm/a lower in tropical South America and ca. 50 mm/a higher in the temperate Andes. Average PLIO
357 temperatures are slightly warmer and LGM temperatures are slightly colder than PI and MH temperatures in tropical
358 and temperate South America (Fig. 8 e and f). These differences are more pronounced in the Andes, however. T_{md} , T_{25}
359 and T_{75} are ca. 5°C higher in the PLIO climate than in PI and MH climates in both temperate and tropical Andes,
360 whereas the same temperatures for the LGM are ca. 2-4°C below PI and MH values (Fig. 8 g and h).

361 For the LGM, the model computes drier-than-PI conditions in tropical South America and tropical Andes,
362 enhanced precipitation in the temperate Andes, and a decrease in temperature that is most pronounced in the Andes. For
363 the PLIO, the model predicts precipitation similar to PI, but with lower precipitation maxima. PLIO temperatures
364 generally increase from PI temperatures, and this increase is most pronounced in the Andes.

365 The climate variability in the region is described by six different clusters (Fig. 9 a-d), which have similar
366 attributes in all time periods. The wettest climate C_1 is also defined by moderate to high precipitation amplitudes, low
367 temperatures and moderate to high u-wind speeds in summer and winter in all time periods (dark blue, Fig. 9 e-h). $C_{2(\text{PI})}$,
368 $C_{2(\text{MH})}$, $C_{3(\text{LGM})}$ and $C_{2(\text{PLIO})}$ are characterized by high temperatures and low seasonal temperature amplitude (dark blue,
369 Fig. 9 e-h), geographically cover the north of the investigated region, and represent a more tropical climate. $C_{5(\text{PI})}$,
370 $C_{5(\text{MH})}$, $C_{6(\text{LGM})}$ and $C_{6(\text{PLIO})}$ are defined by low precipitation and precipitation amplitude, high temperature amplitude and
371 high u-wind speeds in winter (Fig. 9 e-h), cover the low-altitude south of the investigated region (Fig. 9 a-d) and
372 represent dry, extra-tropical climates with more pronounced seasonality. In the PLIO simulation, the lower-altitude east
373 of the region has four distinct climates, whereas the analysis for the other time slice experiments only yield three
374 distinct climates for the same region.

375 376 **3.3.3 Climate change and palaeoclimate characterisation in the St. Elias Range, Southeast Alaska**

377 This section describes the changes in climate and the results from the cluster analysis for South Alaska (Fig. 10-12). As
378 is the case for the other study areas, LGM and PLIO simulations show the largest simulated deviations (Fig. 10b) from
379 PI temperature and precipitation (Fig. 10a). The sign of LGM temperature deviations from PI temperatures is negative
380 and uniform across the region. LGM temperatures are typically 1-9°C below PI temperatures, with the east of the study
381 area experiencing largest cooling. PLIO temperatures are typically 1-5°C above PI temperatures and the warming is

382 uniform for the region. In comparison to the PI simulation, LGM precipitation is lower on land, but higher ($\leq 2300\text{mm}$)
383 in much of the coastal regions of South Alaska. Annual PLIO precipitation is mostly higher ($\leq 800\text{mm}$) than for PI.

384 P_{md} , P_{25} , P_{75} , P_{min} and P_{max} for South Alaskan mean annual precipitation do not differ much between PI, MH and
385 PLIO climates, while P_{md} , P_{25} , P_{75} and P_{min} decrease by ca. 20-40 mm/a and P_{max} increases during the LGM (Fig. 11a).
386 The Alaskan PLIO climate is distinguished from the PI and MH climates by its higher (ca. 2°C) regional temperature
387 means, T_{25} , T_{75} and T_{md} (Fig. 11b). Mean annual temperatures, T_{25} , T_{75} , T_{min} and T_{max} are lower in the LGM than in any
388 other considered time period (Fig. 11b), and about $3\text{-}5^{\circ}\text{C}$ lower than during the PI and MH.

389 Distinct climates are present in the PLIO to PI simulations for Southeast Alaska. Climate cluster C_1 is always
390 geographically restricted to coastal southeast Alaska (Fig. 12 a-d) and characterized by the highest precipitation,
391 precipitation amplitude, temperature, and by relatively low temperature amplitude (dark blue, Fig. 12 e-h). Climate C_2 is
392 characterized by moderate to low precipitation, precipitation amplitude, temperature, and by low temperature amplitude.
393 C_2 is either restricted to coastal southeast Alaska (in MH and LGM climates) or coastal southern Alaska (in PI and
394 PLIO climates). Climate C_3 is described by low precipitation, precipitation amplitude, temperature, and moderate
395 temperature amplitude in all simulations. It covers coastal western Alaska and separates climate C_1 and C_2 from the
396 northern C_4 climate. Climate C_4 is distinguished by the highest mean temperature amplitude, by low temperature and
397 precipitation amplitude, and by lowest precipitation.

398 The geographical ranges of PI climates $C_1\text{-}C_4$ and PLIO climates $C_1\text{-}C_4$ are similar. $C_{1(\text{PI/PLIO})}$ and $C_{2(\text{PI/PLIO})}$ spread
399 over a larger area than $C_{1(\text{MH/LGM})}$ and $C_{2(\text{MH/LGM})}$. $C_{2(\text{PI/PLIO})}$ are not restricted to coastal southeast Alaska, but also cover the
400 coastal southwest of Alaska. The main difference in characterization between PI and PLIO climates $C_1\text{-}C_4$ lies in the
401 greater difference (towards lower values) in precipitation, precipitation amplitude and temperature from $C_{1(\text{PLIO})}$ to
402 $C_{2(\text{PLIO})}$ compared to the relatively moderate decrease in those means from $C_{1(\text{PI})}$ to $C_{2(\text{PI})}$.

403

404 **3.3.4 Climate change and palaeoclimate characterisation in the Cascade Range, US Pacific Northwest**

405 This section describes the character of regional climatology in the US Pacific Northwest and its change over time
406 (Fig. 13-15). The region experiences cooling of typically $9\text{-}11^{\circ}\text{C}$ on land during the LGM, and warming of $1\text{-}5^{\circ}\text{C}$
407 during the PLIO (Fig. 13b) when compared to PI temperatures (Fig. 13a). LGM precipitation increases over water,
408 decreases on land by $\leq 800\text{ mm/a}$ in the North and in the vicinity of Seattle and increases on land by $\leq 1400\text{ mm/a}$ on
409 Vancouver Island, around Portland and the Olympic Mountains, whereas PLIO precipitation does not deviate much
410 from PI values over water and varies in the direction of deviation on land. MH temperature and precipitation deviation
411 from PI values are negligible.

412 P_{md} , P_{25} , P_{75} , P_{min} and P_{max} for the Cascade Range do not notably differ between the four time periods (Fig. 14a).

413 The LGM range of precipitation values is slightly larger than that of the PI and MH with slightly increased P_{md} , while

414 the respective range is smaller for simulation PLIO. The T_{md} , T_{25} , T_{75} and T_{max} values for the PLIO climate are ca. 2°C
415 higher than those values for PI and MH (Fig. 14b). All temperature statistics for the LGM are notably (ca. 13°C) below
416 their analogues in the other time periods (Fig. 14b).

417 PI, LGM and PLIO clusters are similar in both their geographical patterns (Fig. 15 a, c, d) and their
418 characterization by mean values (Fig. 15 e, g, h). C_1 is the wettest cluster and shows the highest amplitude in
419 precipitation. The common characteristics of the C_2 cluster are moderate to high precipitation and precipitation
420 amplitude. C_4 is characterized by the lowest precipitation and precipitation amplitudes, and the highest temperature
421 amplitudes. Regions assigned to clusters C_1 and C_2 are in proximity to the coast, whereas C_4 is geographically restricted
422 to more continental settings.

423 In the PI and LGM climates, the wettest cluster C_1 is also characterized by high temperatures (Fig 10 e, g).
424 However, virtually no grid boxes were assigned to $C_{1(LGM)}$. $C_{1(MH)}$ differs from other climate state's C_1 clusters in that it is
425 also described by moderate to high near surface temperature and temperature amplitude (Fig 10 f), and in that it is
426 geographically less restricted and, covering much of Vancouver Island and the continental coastline north of it (Fig 10
427 b). Near surface temperatures are highest for C_2 in PI, LGM and PLIO climates (Fig 10 e, g, h) and low for $C_{2(MH)}$ (Fig
428 10 f). $C_{2(MH)}$ is also geographically more restricted than C_2 clusters in PI, LGM and PLIO climates (Fig 10 a-d). $C_{2(PI)}$,
429 $C_{2(MH)}$ and $C_{2(LGM)}$ have a low temperature amplitude (Fig 10 e-g), whereas $C_{2(PLIO)}$ is characterized by a moderate
430 temperature amplitude (Fig 10 h).

431

432 **4. Discussion**

433 In the following, we synthesise our results and compare to previous studies that investigate the effects of
434 temperature and precipitation change on erosion. Since our results do not warrant merited discussion of subglacial
435 processes without additional work that is beyond the scope of this study, we instead advise caution in interpreting the
436 presented precipitation and temperature results in an erosional context where the regions are covered with ice. For
437 convenience, ice cover is indicated on figures 2,3,4,7,10 and 13, and a summary of ice cover used as boundary
438 conditions for the different time slice experiments is included in the supplemental material. Where possible, we relate
439 the magnitude of climate change predicted in each geographical study area with terrestrial proxy data.

440

441 **4.1 Synthesis of temperature changes**

442

443 **4.1.1 Temperature changes and implications for weathering and erosion**

444 Changes in temperature can affect physical weathering due to temperature-induced changes in periglacial
445 processes and promote frost cracking and frost creep [e.g., Matsuoka, 2001; Schaller et al., 2002; Matsuoka and

446 Murton, 2008; Delunel et al., 2010; Andersen et al., 2015; Marshall et al., 2015], and also biotic weathering and erosion
447 [e.g. Moulton et al., 1998; Banfield et al., 1999; Dietrich and Perron, 2006]. Quantifying and understanding past
448 changes in temperature is thus vital for our understanding of denudation histories. In the following, we highlight regions
449 in the world where future observational studies might be able to document significant warming or cooling that would
450 influence temperature related changes in physical and chemical weathering over the last ~3 Ma.

451 Simulated MH temperatures show little deviation (typically $< 1^{\circ}\text{C}$) from PI temperatures in the investigated
452 regions (Fig. 2b), suggesting little difference in MH temperature-related weathering. The LGM experiences widespread
453 cooling, which is accentuated at the poles. , increasin the equator-to-pole pressure gradient and consequently
454 strengthens global atmospheric circulation. Despite this global trend, cooling in coastal South Alaska is higher ($\leq 9^{\circ}\text{C}$)
455 than in central Alaska ($0\pm 1^{\circ}\text{C}$). The larger temperature difference in South Alaska geographically coincides with ice
456 cover (Fig. 10b), and should thus be interpreted in context of a different erosional regime. Cooling in most of the lower-
457 latitude regions in South America and central to southeast Asia is relatively mild. The greatest temperature differences
458 in South America are observed for western Patagonia, which was mostly covered by glaciers. The Tibetan plateau
459 experiences more cooling ($3\text{-}5^{\circ}\text{C}$) than adjacent low-altitude regions ($1\text{-}3^{\circ}\text{C}$) during the LGM.

460 The PLIO simulation is generally warmer, and temperature differences are accentuated warming at the poles.
461 Warming in simulation PLIO is greatest in parts of Canada, Greenland and Antarctica (up to 19°C), which
462 geographically coincides with the presence of ice in the PI reference simulation and thus may be attributed to
463 differences in ice cover. It should therefore also be regarded as areas in which process domain shifted from glacial to
464 non-glacial. The warming in simulation PLIO in South Alaska and the US Pacific northwest is mostly uniform and in
465 the range of $1\text{-}5^{\circ}\text{C}$. As before, changes in ice cover reveal that the greatest warming may be associated with the absence
466 of glaciers relative to the PI simulation. Warming in South America is concentrated at the Pacific west coast and the
467 Andes between Lima and Chiclayo, and along the Chilean-Argentinian Andes south of Bolivia ($\leq 9^{\circ}\text{C}$).

468 Overall, annual mean temperatures in the MH simulation show little deviation from PI values. The more
469 significant temperature deviations of the colder LGM and of the warmer PLIO simulations are accentuated at the poles
470 leading to higher and lower equator-to-pole temperature gradients respectively. The largest temperature-related changes
471 (relative to PI conditions) in weathering and subsequent erosion, in many cases through a shift in the process domain
472 from glacial to non-glacial or vice versa, are therefore to be expected in the LGM and PLIO climates.

473

474 **4.1.2 Temperature comparison to other studies**

475 LGM cooling is accentuated at the poles, thus increases the equator-to-pole pressure gradient and consequently
476 strengthens global atmospheric circulation, and is in general agreement with studies such as Otto-Bliesner et al. [2006]
477 and Braconnot et al. [2007]. The PLIO simulation shows little to no warming in the tropics and accentuated warming at

478 the poles, as do findings of Salzmann et al. [2011] and Robinson [2009] and Ballantyne [2010] respectively. This would
479 reduce the equator-to-pole sea and land surface temperature gradient, as also reported by Dowsett et al. [2010], and also
480 weaken global atmospheric circulation. Agreement with proxy-based reconstructions, as is the case of the relatively
481 little warming in lower latitudes, is not surprising given that sea surface temperature reconstructions (derived from
482 previous coarse resolution coupled ocean-atmosphere models) are prescribed in this uncoupled atmosphere simulation.
483 It should be noted that coupled ocean-atmosphere simulations do predict more low-latitude warming [e.g. Stepanek and
484 Lohmann 2012; Zhang et al. 2013b]. The PLIO warming in parts of Canada and Greenland (up to 19°C) and consistent
485 with values based on multi-proxy studies [Ballantyne et al., 2010]. Due to a scarcity of palaeobotanical proxies in
486 Antarctica, reconstruction-based temperature and ice-sheet extent estimates for a PLIO climate have high uncertainties
487 [Salzmann et al., 2011], making model validation difficult. Furthermore, controversy about relatively little warming in
488 the south polar regions compared to the north polar regions remains [e.g. Hillenbrand and Fütterer, 2002; Wilson et al.,
489 2002]. Mid-latitude PLIO warming is mostly in the 1-3°C range with notable exceptions of cooling in the northern
490 tropics of Africa and on the Indian subcontinent, especially south of the Himalayan orogen.

491

492 **4.2 Synthesis of precipitation changes**

493

494 **4.2.1 Precipitation and implications for weathering and erosion**

495 Changes in precipitation affects erosion through river incision, sediment transport, and erosion due to extreme
496 precipitation events and storms [e.g. Whipple and Tucker, 1999; Hobbey et al., 2010]. Furthermore, vegetation type and
497 cover also co-evolve with variations in precipitation and with changes in geomorphology [e.g. Marston 2010; Roering
498 et al., 2010]. These vegetation changes in turn modify hillslope erosion by increasing root mass and canopy cover, and
499 decreasing water-induced erosion via surface runoff [e.g. Gyssels et al., 2005]. Therefore, understanding and
500 quantifying changes in precipitation in different palaeoclimates is necessary for a more complete reconstruction of
501 orogen denudation histories. A synthesis of predicted precipitation changes is provided below, and highlights regions
502 where changes in river discharge and hillslope processes might be impacted by climate change over the last ~3 Ma.

503 Most of North Africa is notably wetter during the MH, which is characteristic of the African Humid Period
504 [Sarnthein 1978]. This pluvial regional expression of the Holocene Climatic Optimum is attributed to sudden changes in
505 the strength of the African monsoon caused by orbital-induced changes in summer insolation [e.g. deMenocal et al.
506 2000]. Southern Africa is characterised by a wetter climate to the east and drier climate to the west of the approximate
507 location of the Congo Air Boundary (CAB), the migration of which has previously been cited as a cause for
508 precipitation changes in East Africa [e.g. Juninger et al. 2014]. In contrast, simulated MH precipitation rates show little
509 deviation from the PI in most of the investigated regions, suggesting little difference in MH precipitation-related

510 erosion. The Himalayan orogen is an exception and shows a precipitation increase of up to 2000 mm/a. The climate's
511 enhanced erosion potential, that could result from such a climatic change, should be taken into consideration when
512 palaeo-erosion rates estimated from the geological record in this area are interpreted [e.g. Bookhagen et al., 2005].
513 Specifically, higher precipitation rates (along with differences in other rainfall-event parameters) could increase the
514 probability of mass movement events on hillslopes, especially where hillslopes are close to the angle of failure [e.g.
515 Montgomery, 2001], and modify fluxes to increase shear stresses exerted on river beds and increase stream capacity to
516 enhance erosion on river beds (e.g. by abrasion).

517 Most precipitation on land is decreased during the LGM due to large-scale cooling and decreased evaporation
518 over the tropics, resulting in an overall decrease in inland moisture transport [e.g., Braconnot et al. 2007]. North
519 America, south of the continental ice sheets, is an exception and experiences increases in precipitation. For example, the
520 investigated US Pacific Northwest and the southeastern coast of Alaska experience experience strongly enhanced
521 precipitation of ≤ 1700 mm/a and ≤ 2300 mm/a, respectively. These changes geographically coincide with differences in
522 ice extent. An increase in precipitation in these regions may have had direct consequences on the glaciers' mass balance
523 and equilibrium line altitudes, where the glaciers' effectiveness in erosion is highest [e.g. Egholm et al., 2009; Yanites
524 and Ehlers, 2012]. The differences in the direction of precipitation changes, and accompanying changes in ice cover
525 would likely result in more regionally differentiated variations in precipitation-specific erosional processes in the St.
526 Elias Range rather than causing systematic offsets for the LGM. Although precipitation is significantly reduced along
527 much of the Himalayan orogen (≤ 1600 mm/a), northeast India experiences strongly enhanced precipitation (≤ 1900
528 mm/a). This could have large implications for studies of uplift and erosion at orogen syntaxes, where highly localized
529 and extreme denudation has been documented [e.g. Koons et al., 2013; Bendick and Ehlers, 2014].

530 Overall, the PLIO climate is wetter than the PI climate, in particular in the (northern) mid-latitudes, and possibly
531 related to a northward shift of the northern Hadley cell boundary that is ultimately the result of a reduced equator-to-
532 pole temperature gradient [e.g. Haywood et al. 2000, 2013; Dowsett et al. 2010]. Most of the PLIO precipitation over
533 land increases, esp. at the Himalayan orogen by ≤ 1400 mm/a, and decreases from eastern Nepal to Namcha Barwa
534 (≤ 2500 mm/a). Most of the Atacama Desert experiences an increase in precipitation by 100-200 mm/a, which may have
535 to be considered in erosion and uplift history reconstructions for the Andes. A significant increase (~ 2000 mm/a) in
536 precipitation from simulation PLIO to modern conditions is simulated for the eastern margin of the Andean Plateau in
537 Peru and for northern Bolivia. This is consistent with recent findings of a pulse of canyon incision in these locations in
538 the last ~ 3 Ma [Lease and Ehlers, 2013].

539 Overall, the simulated MH precipitation varies least from PI precipitation. The LGM is generally drier than the
540 PI simulation, even though pockets of a wetter-than-PI climate do exist, such as much of coastal North America. Extra-
541 tropical increased precipitation of the PLIO simulation and decreased precipitation of the LGM climate may be the

542 result of decreased and increased equator-to-pole temperature gradients, respectively.

543

544 **4.2.2 Precipitation comparison to other studies**

545 The large scale LGM precipitation decrease on land, related to cooling and decreased evaporation over the
546 tropics, and greatly reduced precipitation along much of the Himalayan orogeny, is consistent with previous studies by,
547 (for example) Braconnot et al. [2007]. The large scale PLIO precipitation increase due to a reduced equator-to-pole
548 temperature gradient, has previously been pointed out by e.g. Haywood et al. [2000, 2013] and Dowsett et al. [2010]. A
549 reduction of this gradient by ca. 5°C is indeed present in the PLIO simulation of this study (Fig. 2b). This precipitation
550 increase over land agrees well with simulations performed at a lower spatial model resolution [cf. Stepanek and
551 Lohmann, 2012]. Section 4.4 includes a more in-depth discussion of how simulated MH and LGM precipitation
552 differences compare with proxy-based reconstructions in South Asia and South America.

553

554 **4.3 Trends in Late Cenozoic changes in regional climatology**

555 This section describes the major changes in regional climatology and highlights their possible implications on
556 erosion rates.

557

558 *Himalaya-Tibet, South Asia*

559 In South Asia, cluster-analysis based categorization and description of climates (Fig. 6) remains similar
560 throughout time. However, the two wettest climates (C₁ and C₂) are geographically more restricted to the eastern
561 Himalayan orogen in the LGM simulation. Even though precipitation over the South Asia region is generally lower, this
562 shift indicates that rainfall on land is more concentrated in this region and that the westward drying gradient along the
563 orogen is more accentuated than during other time periods investigated here. While there is limited confidence in the
564 global Atmospheric General Circulation Model's abilities to accurately represent meso-scale precipitation patterns [e.g.
565 Cohen 1990], the simulation warrants careful consideration of possible, geographically non-uniform offsets in
566 precipitation in investigations of denudation and uplift histories.

567 MH precipitation and temperature in tropical, temperate and high-altitude South Asia is similar to PI
568 precipitation and temperature, whereas LGM precipitation and temperatures are generally lower (by ca. 100 mm/a and
569 1-2°C respectively), possibly reducing precipitation-driven erosion and enhancing frost-driven erosion in areas pushed
570 into a near-zero temperature range during the LGM.

571

572 *Andes, South America*

573 Clusters in South America (Fig. 9), which are somewhat reminiscent of the Köppen and Geiger classification

574 [Kraus, 2001], remain mostly the same over the last 3 Ma. In the PLIO simulation, the lower-altitude east of the region
575 is characterized by four distinct climates, which suggests enhanced latitudinal variability in the PLIO climate compared
576 to PI with respect to temperature and precipitation.

577 The largest temperature deviations from PI values are derived for the PLIO simulation in the (tropical and
578 temperate) Andes, where temperatures exceed PI values by 5°C. On the other hand, LGM temperatures in the Andes are
579 ca. 2-4°C below PI values in the same region (Fig 7 g and h). In the LGM simulation, tropical South America
580 experiences ca. 50 mm/a less precipitation, the temperate Andes receive ca. 50 mm/a more precipitation than in PI and
581 MH simulations. These latitude-specific differences in precipitation changes ought to be considered in attempts to
582 reconstruct precipitation-specific palaeoerosion rates in the Andes on top of longitudinal climate gradients highlighted
583 by, e.g., Montgomery et al. [2001].

584

585 *St. Elias Range, South Alaska*

586 South Alaska is subdivided into two wetter and warmer clusters in the south, and two drier, colder clusters in the
587 north. The latter are characterised by increased seasonal temperature variability due to being located at higher latitudes
588 (Fig. 12). The different equator-to-pole temperature gradients for LGM and PLIO may affect the intensity of the Pacific
589 North American Teleconnection (PNA) [Barnston and Livzey, 1987], which has significant influence on temperatures
590 and precipitation, especially in southeast Alaska, and may in turn result in changes in regional precipitation and
591 temperature patterns and thus on glacier mass balance. Changes in the Pacific Decadal Oscillation, which is related to
592 the PNA pattern, has previously been connected to differences in Late Holocene precipitation [Barron and Anderson,
593 2011]. While this climate cluster pattern appears to be a robust feature for the considered climate states, and hence over
594 the recent geologic history, the LGM sets itself apart from PI and MH climates by generally lower precipitation (20-40
595 mm) and lower temperatures (3-5°C, Fig. 10, 11), which may favour frost driven weathering during glacial climate
596 states [e.g. Andersen et al., 2015; Marshall et al. 2015] in unglaciated areas, whereas glacial processes would have
597 dominated most of this region as it was covered by ice. Simulation PLIO is distinguished by temperatures that exceed
598 PI and MH conditions by ca. 2°C, and by larger temperature and precipitation value ranges, possibly modifying
599 temperature- and precipitation-dependent erosional processes in the region of South Alaska.

600

601 *Cascade Range, US Pacific Northwest*

602 In all time slices, the geographic climate patterns, based on the cluster analysis (Fig. 15), represents an increase
603 in the degree of continentality from the wetter coastal climates to the further inland located climates with greater
604 seasonal temperature amplitude and lower precipitation and precipitation amplitude (Fig 15 e-h). The most notable
605 difference between the time slices is the strong cooling during the LGM, when temperatures are ca. 13°C (Fig. 13, 14)

606 below those of other time periods. Given that the entire investigated region was covered by ice (Fig 13), we can assume
607 a shift to glacially dominated processes.

608

609 **4.4 Comparison of simulated and observed precipitation differences**

610 The predicted precipitation differences reported in this study were compared with observed (proxy record)
611 palaeoprecipitation change. Proxy based precipitation reconstructions for the MH and LGM are presented for South
612 Asia and South America for the purpose of assessing ECHAM5 model performance, and for identifying inconsistencies
613 between neighbouring proxy data. Due to the repeated glaciations, detailed terrestrial proxy records for the time slices
614 investigated here are not available, to the best of our knowledge, for the Alaskan and Pacific NW USA studies.
615 Although marine records and records of glacier extent are available in these regions, the results from them do not
616 explicitly provide estimates of wetter/drier, or colder/warmer conditions that can be spatially compared to the
617 simulation estimates. For these two areas with no available records, the ECHAM5 predicted results therefore provide
618 predictions from which future studies can formulate testable hypotheses to evaluate.

619 The palaeoclimate changes in terrestrial proxy records compiled here are reported as “wetter than today”, “drier
620 than today” or “the same as today” for each of the study locations, and plotted on top of the simulation-based difference
621 maps as upward facing blue triangles, downward facing red triangles and grey circles respectively (Fig. 16, 17). The
622 numbers listed next to those indicators are the ID numbers assigned to the studies compiled for this comparison and are
623 associated with a citation provided in the figure captions.

624 In South Asia, 14/26 results from local studies agree with the model predicted precipitation changes for the MH.
625 The model seems able to reproduce the predominantly wetter conditions on much of the Tibetan plateau, but predicts
626 slightly drier conditions north of Chengdu, which is not reflected in local reconstructions. The modest mismatch
627 between ECHAM5 predicted and proxy-based MH climate change in south Asia was also documented by Li et al.,
628 [2017], whose simulations were conducted at a coarser (T106) resolution. Despite these model-proxy differences, we
629 note that there are significant discrepancies between the proxy data themselves in neighbouring locations in the MH,
630 highlighting caution in relying solely upon these data for regional palaeoclimate reconstructions. These differences
631 could result from either poor age-constraints in the reported values, or systematic errors in the transfer functions used to
632 convert proxy measurements to palaeoclimate conditions. The widespread drier conditions on the Tibetan Plateau and
633 immediately north of Laos are confirmed by 7/7 of the palaeoprecipitation reconstructions. 23/39 of the reconstructed
634 precipitation changes agree with model predictions for South America during the MH. The model predicted wetter
635 conditions in the central Atacama desert, as well as the drier conditions northwest of Santiago are confirmed by most of
636 the reconstructions. The wetter conditions in southernmost Peru and the border to Bolivia and Chile cannot be
637 confirmed by local studies. 11/17 of the precipitation reconstructions for the LGM are in agreement with model

638 predictions. These include wetter conditions in most of Chile. The most notable disagreement can be seen in northeast
639 Chile at the border to Argentina and Bolivia, where model predicted wetter conditions are not confirmed by reported
640 reconstructions from local sites.

641 Model performance is, in general, higher for the LGM than for the MH and overall satisfactory given that it
642 cannot be expected to resolve sub-grid scale differences in reported palaeoprecipitation reconstructions. However, as
643 mentioned above, it should be noted that some locations (MH of south Asia, and MH of norther Chile) discrepancies
644 exist between neighbouring proxy samples and highlight the need for caution in how these data are interpreted. Other
645 potential sources of error resulting in disagreement of simulated and proxy-based precipitation estimates are the model's
646 shortcomings in simulating orographic precipitation at higher resolutions, and uncertainties in palaeoclimate
647 reconstructions at the local sites. In summary, although some differences are evident in both the model-proxy data
648 comparison and between neighbouring proxy data themselves, the above comparison highlights an overall good
649 agreement between the model and data for the south Asia and South American study areas. Thus, although future
650 advances in GCM model parameterisations and new or improved palaeoclimate proxy techniques are likely, the
651 palaeoclimate changes documented here are found to be in general robust and provide a useful framework for future
652 studies investigating how these predicted changes in palaeoclimate impact denudation.

653

654 **4.5 Conclusions**

655 We present a statistical cluster-analysis-based description of the geographic coverage of possible distinct
656 regional expressions of climates from four different time slices (Fig. 6, 9, 12, 15). These are determined with respect to
657 a selection of variables that characterize the climate of the region and may be relevant to weathering and erosional
658 processes. While the geographic distribution of climate remains similar throughout time (as indicated by results of four
659 different climate states representative for the climate of the last 3 Ma), results for the PLIO simulation suggests more
660 climatic variability east of the Andes (with respect to near-surface temperature, seasonal temperature amplitude,
661 precipitation, seasonal precipitation amplitude and seasonal u-wind and v-wind speeds). Furthermore, the wetter
662 climates in the South Asia region retreat eastward along the Himalayan orogen for the LGM simulation, this is due to
663 decreased precipitation along the western part of the orogen and enhanced precipitation on the eastern end, possibly
664 signifying more localised high erosion rates.

665 Most global trends of the high-resolution LGM and PLIO simulations conducted here are in general agreement
666 with previous studies [Otto-Bliesner et al., 2006; Braconnot et al., 2007; Wei and Lohmann, 2012; Lohmann et al.,
667 2013; Zhang et al., 2013b, 2014; Stepanek and Lohmann, 2012]. The MH does not deviate notably from the PI, the
668 LGM is relatively dry and cool, while the PLIO is comparably wet and warm. While the simulated regional changes in
669 temperature and precipitation usually agree with the sign (or direction) of the simulated global changes, there are

670 region-specific differences in the magnitude and direction. For example, the LGM precipitation of the Tropical Andes
671 does not deviate significantly from PI precipitation, whereas LGM precipitation in the Temperate Andes is enhanced.

672 Comparisons to local, proxy-based reconstructions of MH and LGM precipitation in South Asia and South
673 America reveal satisfactory performance of the model in simulating the reported differences. The model performs better
674 for the LGM than the MH. We note however that compilations of proxy data such as we present here, also identify
675 inconsistencies between neighbouring proxy data themselves, warranting caution in the extent to which both proxy data
676 and palaeoclimate models are interpreted for MH climate change in south Asia, and western South America.

677 The changes in regional climatology presented here are manifested, in part, by small to large magnitude changes
678 in fluvial and hillslope relevant parameters such as precipitation and temperature. For the regions investigated here we
679 find that precipitation differences between the PI, MH, LGM, and PLIO are in many areas around +/- 200-600 mm/yr,
680 and locally can reach maximums of +/- 1000-2000 mm/yr (Figs. 4, 7, 10, 13). In areas where significant precipitation
681 increases are accompanied by changes in ice extent, such as parts of southern Alaska during the LGM, we would expect
682 a shift in the erosional regime to glacier dominated processes. Temperature differences between these same time periods
683 are around 1-4 °C in many places, but reach maximum values of 8-10 °C. Many of these maxima in the temperature
684 differences geographically coincide with changes in ice sheet extent and must therefore be interpreted as part of a
685 different erosional process domains. However, we also observe large temperature differences (~5°C) in unglaciated
686 areas that would be affected by hillslope, frost cracking, and fluvial processes. The magnitude of these differences are
687 not trivial, and will likely impact fluvial and hillslope erosion and sediment transport, as well as biotic and abiotic
688 weathering. The regions of large magnitude changes in precipitation and temperature documented here (Figs. 4, 7, 10,
689 13) offer the highest potential for future observational studies interested in quantifying the impact of climate change on
690 denudation and weathering rates.

691

692

693 **Acknowledgements**

694 The model simulations presented in this study are freely available to interested persons by contacting S. Mutz or T.
695 Ehlers. We note however that the data files are very large (~4 TB, and too large to archive in journal supplementary
696 material) and require familiarity in reading/plotting NetCDF formatted files. European Research Council (ERC)
697 Consolidator Grant number 615703 provided support for S. Mutz. Additional support is acknowledged from the
698 German science foundation (DFG) priority research program 1803 (EarthShape: Earth Surface Shaping by Biota; grants
699 EH329/14-1 and EH329/17-1). We thank B. Adams and J. Starke for constructive discussions. The DKRZ is thanked
700 for computer time used for some of the simulations presented here. C. Stepanek, M. Werner, and G. Lohmann

701 acknowledge funding by the Helmholtz Climate Initiative Reklim and the Alfred Wegener Institute's research
702 programme Marine, Coastal and Polar Systems.

703

704

705 **Figure Captions**

706

707 **Figure 1** Topography for regions (a) tropical South Asia, (b) temperate South Asia, (c) high altitude South Asia, (d)
708 temperate South America, (e) tropical South America, (f) temperate Andes, (g) tropical Andes, SE Alaska and Cas-
709 cadia.

710 **Figure 2** Global PI annual mean near-surface temperatures (a), and deviations of MH, LGM and PLIO annual mean
711 near-surface temperatures from PI values (b). Units are °C and insignificant ($p < 99\%$) differences (as determined by
712 a t-test) are greyed out.

713 **Figure 3** Global PI annual mean precipitation (a), and deviations of MH, LGM and PLIO annual mean near-surface
714 temperatures from PI values (b). Units are mm/yr.

715 **Figure 4** PI annual mean near-surface temperatures (a), and deviations of MH, LGM and PLIO annual mean near-sur-
716 face temperatures from PI values (b) for the South Asia region. Insignificant ($p < 99\%$) differences (as determined
717 by a t-test) are greyed out.

718 **Figure 5** PI, MH, LGM and PLIO annual mean precipitation in (a) tropical South Asia, (b) temperate South Asia, and
719 (c) high-altitude South Asia; PI, MH, LGM and PLIO annual mean temperatures in (d) tropical South Asia, (e) tem-
720 perate South Asia, and (f) high-altitude South Asia. For each time slice, the minimum, lower 25th percentile, median,
721 upper 75th percentile and maximum are plotted.

722 **Figure 6** Geographical coverage and characterization of climate classes C_1 - C_6 based on cluster-analysis of 8 variables
723 (near surface temperature, seasonal near surface temperature amplitude, total precipitation, seasonal precipitation
724 amplitude, u-wind in January and July, v-wind in January and July) in the South Asia region. The geographical cov-
725 erage of the climates C_1 - C_6 is shown on the left for PI (a), MH (b), LGM (c) and PLIO (d); the complementary,
726 time-slice specific characterization of C_1 - C_6 for PI (e), MH (f), LGM (g) and PLIO (h) is shown on the right.

727 **Figure 7** PI annual mean near-surface temperatures (a), and deviations of MH, LGM and PLIO annual mean near-sur-
728 face temperatures from PI values (b) for western South America. Insignificant ($p < 99\%$) differences (as determined

729 by a t-test) are greyed out.

730 **Figure 8** PI, MH, LGM and PLIO annual mean precipitation in (a) tropical South America, (b) temperate South Amer-
731 ica, (c) tropical Andes, and (d) temperate Andes; PI, MH, LGM and PLIO annual mean temperatures in (e) tropical
732 South America, (f) temperate South America, (g) tropical Andes, and (h) temperate Andes. For each time slice, the
733 minimum, lower 25th percentile, median, upper 75th percentile and maximum are plotted.

734 **Figure 9** Geographical coverage and characterization of climate classes C₁- C₆ based on cluster-analysis of 8 variables
735 (near surface temperature, seasonal near surface temperature amplitude, precipitation, seasonal precipitation amp-
736 litude, u-wind in January and July, v-wind in January and July) in western South America. The geographical cover-
737 age of the climates C₁- C₆ is shown on the left for PI (a), MH (b), LGM (c) and PLIO (d); the complementary, time-
738 slice specific characterization of C₁- C₆ for PI (e), MH (f), LGM (g) and PLIO (h) is shown on the right.

739 **Figure 10** PI annual mean near-surface temperatures (a), and deviations of MH, LGM and PLIO annual mean near-sur-
740 face temperatures from PI values (b) for the South Alaska region. Insignificant ($p < 99\%$) differences (as determined
741 by a t-test) are greyed out.

742 **Figure 11** PI, MH, LGM and PLIO annual mean precipitation (a), and mean annual temperatures (b) in South Alaska.
743 For each time slice, the minimum, lower 25th percentile, median, upper 75th percentile and maximum are plotted.

744 **Figure 12** Geographical coverage of climate classes C₁- C₄ based on cluster-analysis of 4 variables (near surface tem-
745 perature, seasonal near surface temperature amplitude, total precipitation, seasonal total precipitation amplitude) in
746 southern Alaska. The geographical coverage of the climates C₁- C₄ is shown on the left for PI (a), MH (b), LGM (c)
747 and PLIO (d); the complementary, time-slice specific characterization of C₁- C₆ for PI (e), MH (f), LGM (g) and
748 PLIO (h) is shown on the right.

749 **Figure 13** PI annual mean near-surface temperatures (a), and deviations of MH, LGM and PLIO annual mean near-sur-
750 face temperatures from PI values (b) for the US Pacific Northwest. Insignificant ($p < 99\%$) differences (as determ-
751 ined by a t-test) are greyed out.

752 **Figure 14** PI, MH, LGM and PLIO annual mean precipitation (a), and annual mean temperatures (b) in the Cascades,
753 US Pacific Northwest. For each time slice, the minimum, lower 25th percentile, median, upper 75th percentile and
754 maximum are plotted.

755 **Figure 15** Geographical coverage and characterization of climate classes C₁- C₄ based on cluster-analysis of 4 variables

756 (near surface temperature, seasonal near surface temperature amplitude, total precipitation, seasonal total precipita-
757 tion amplitude) in the Cascades, US Pacific Northwest. The geographical coverage of the climates C₁- C₄ is shown
758 on the left for PI (a), MH (b), LGM (c) and PLIO (d); the complementary, time-slice specific characterization of C₁-
759 C₆ for PI (e), MH (f), LGM (g) and PLIO (h) is shown on the right.

760 **Figure 16** Simulated annual mean precipitation deviations of MH (left) and LGM (right) from PI values in South Asia,
761 and temporally corresponding proxy-based reconstructions, indicating wetter (upward facing blue triangles), drier
762 (downward facing red triangles) or similar (grey circles) conditions in comparison with modern climate. MH proxy-
763 based precipitation differences are taken from Mügler et al. (2010) (66), Wischnewski et al. (2011) (67), Mischke et
764 al. (2008), Wischnewski et al. (2011), Herzsuh et al. (2009) (68), Yanhong et al. (2006) (69), Morrill et al. (2006)
765 (70), Wang et al. (2002) (71), Wuennemann et al. (2006) (72), Zhang et al. (2011), Morinaga et al. (1993),
766 Kashiwaya et al. (1995) (73), Shen et al. (2005) (74), Liu et al. (2014) (75), Herzsuh et al. (2006) (76), Zhang and
767 Mischke (2009) (77), Nishimura et al. (2014) (78), Yu and Lai (2014) (79), Gasse et al. (1991) (80), Van Campo et
768 al. (1996) (81), Demske et al. (2009) (82), Kramer et al. (2010) (83), Herzsuh et al. (2006) (84), Hodell et al.
769 (1999)(85), Hodell et al. (1999) (86), Shen et al. (2006) (87), Tang et al. (2000) (88), Tang et al. (2000) (89), Zhou
770 et al. (2002) (90), Liu et al. (1998) (91), Asashi (2010)(92), Kotila et al. (2009) (93), Kotila et al. (2000) (94), Wang
771 et al. (2002) (95), Hu et al. (2014) (96), Hodell et al. (1999) (97), Hodell et al. (1999) (98).

772 **Figure 17** Simulated annual mean precipitation deviations of MH (left) and LGM (right) from PI values in South Amer-
773 ica, and temporally corresponding proxy-based reconstructions, indicating wetter (upward facing blue triangles),
774 drier (downward facing red triangles) or similar (grey circles) conditions in comparison with modern climate. MH
775 proxy-based precipitation differences are taken from Bird et al. (2011) (1), Hansen et al (1994) (2), Hansen et al
776 (1994) (3), Hansen et al (1994) (4), Hansen et al (1994) (5), Hansen et al (1994) (6), Hillyer et al. (2009) (7),
777 D'Agostino et al. (2002) (8), Baker et al. (2001) (9), Schwalb et al (1999) (10), Schwalb et al (1999) (11), Schwalb
778 et al (1999) (12), Schwalb et al (1999) (13), Moreno et al (2009) (14), Pueyo et al (2011) (15), Mujica et al (2015)
779 (16), Fritz et al. (2004) (17), Gayo et al. (2012) (18), Latorre et al. (2006) (19), Latorre et al. (2003) (20), Quade et al
780 (2008) (21), Bobst et al. (2001) (22), Grosjean et al. (2001) (23), Betancourt et al. (2000) (24), Latorre et al. (2002)
781 (25), Rech et al. (2003) (26), Diaz et al. (2012) (27), Maldonado et al (2005) (28), Diaz et al. (2012) (29), Lamy et
782 al. (2000) (30), Kaiser et al. (2008) (31), Maldonado et al. (2010) (32), Villagrán et al. (1990) (33), Méndez et al.
783 (2015) (34), Maldonado et al. (2006) (35), Lamy et al. (1999) (36), Jenny et al. (2002) (37), Jenny et al. (2002b)
784 (38), Villa-Martínez et al. (2003) (39), Bertrand et al. (2008) (40), De Basti et al. (2008) (41), Lamy et al. (2009)
785 (42), Lamy et al. (2002) (43), Szeicz et al. (2003) (44), de Porras et al. (2012) (45), de Porras et al. (2014) (46),

786 Markgraf et al. (2007) (47), Siani et al. (2010) (48), Gilli et al. (2001) (49), Markgraf et al. (2003) (50), Stine et al.
787 (1990) (51).

788

789

790 **References**

791

792 Abe-Ouchi, A., Saito, F., Kageyama, M., Bracannot, P., Harrison, S. P., Lambeck, K., Otto-Bliesner, B. L., Peltier,
793 W.R., Tarasov, L., Peterschmitt, J.-Y., Takahashi, K.: Ice-sheet configuration in the CMUP5/PMIP3 Last Glacial
794 Maximum experiments. *Geosci. Model Dev.*, 8, 3621-3637, doi:10.5194/gmd-8-3621-2015, 2015

795 Andersen, J., Egholm, D.L., Knudsen, M.F., Jansen, J., Nielsen, S.B., The periglacial engine of mountain erosion – Part
796 1: Rates of frost cracking and frost creep., *Earth Surface Dynamics*, 3(4), 447-462, 2015.

797 Arnold, L., Breon, F.M., and Brewer, S: The earth as an extrasolar planet: the vegetation spectral signature today and
798 during the last Quaternary climatic extrema, *Int. J. Astrobiol.*, 8, 81–94. [http://dx.doi.org/10.1017/](http://dx.doi.org/10.1017/S1473550409004406)
799 [S1473550409004406](http://dx.doi.org/10.1017/S1473550409004406), 2009.

800 Asahi, K.: Equilibrium-line altitudes of the present and Last Glacial Maximum in the eastern Nepal
801 Himalayas and their implications for SW monsoon climate, *Quatern. Int.*, 212, 26-34,
802 doi:10.1016/j.quaint.2008.08.004, 2010.

803 Bahrenberg , G., Giese, E., and Nipper, J.: Multivariate Statistik. *Statistische Methoden in der Geographie 2*, Stuttgart,
804 1992.

805 Baker, P. A., Seltzer, G. O., Fritz, S. C., Dunbar, R. B., Grove, M. J., Tapia, P. M., Cross L., Rowe H. D., and
806 Baroda, J. P.: The History of South America Tropical Precipitation for the Past 25,000 Years, *Earth and*
807 *Atmospheric Sciences*, 291, 640-643, doi:10.1126/science.291.5504.640, 2001.

808 Ballantyne, A.P., Greenwood, D.R., Sinninghe Damste, J.S., Csank, A.Z., Eberle, J.J., and Rybczynski, N.:
809 Significantly warmer Arctic surface temperatures during the Pliocene indicated by multiple independent proxies,
810 *Geology* 38 (7), 603–606, 2010.

811 Banfield, J.F., Barker, W.W., Welch, S.A., and Taunton, A.: Biological impact on mineral dissolution: application of
812 the lichen model to understanding mineral weathering in the rhizosphere, *Proceedings of the National Academy of*
813 *Sciences*, 96, 3404-3411, 1999.

814 Barnston, A. G. and Livezey, R. E.: Classification, Seasonality and Persistence of Low-Frequency
815 Atmospheric Circulation Patterns, *Mon. Weather Rev.*, 115, 1083-1126, doi:10.1175/1520-
816 0493(1987)1151083:CSAPOL2.0.CO;2, 1987.

817 Barron, J.A., and Anderson, L.: Enhanced Late Holocene ENSO/PDO expression along the margins of the

- 818 eastern North Pacific. *Quaternary International*, 235, 3-12, 2011.
- 819 Bendick, R., and Ehlers, T.A.: Extreme localized exhumation at syntaxes initiated by subduction geometry, *Geophys.*
820 *Res. Lett.*, 41(16), 2014GL061026, doi:10.1002/2014GL061026, 2014.
- 821 Bertrand, S., Charlet F., Charlier B., Renson V., and Fagel N.: Climate variability of southern Chile since the
822 Last Glacial Maximum: a continuous sedimentological records from Lago Puyehue (40°S), *J. Paleolimnol.*,
823 39, 179-195, doi:10.1007/s10933-007-9117-y, 2008.
- 824 Betancourt, J. L., Latorre C., Rech J. A., Quade J., and Rylander K.A.: A 22,000 Year Record of Monsoonal
825 Precipitation from Northern Chile's Atacama Desert, *Science*, 289, 1542-1546, doi: 10.1126/
826 science.289.5484.1542, 2000.
- 827 Bigelow, N. H., Brubaker, L. B., Edwards, M. E., Harrison, S. P., Prentice, I. C., Anderson, P. M., Andreev, A. A.,
828 Bartlein, P. J., Christensen, T. R., Cramer, W., Kaplan, J. O., Lozhkin, A. V., Matveyeva, N. V., Murray, D. V.,
829 McGuire, A. D., Razzhivin, V. Y., Ritchie, J. C., Smith, B., Walker, D. A., Gajewski, K., Wolf, V., Holmqvist, B.
830 H., Igarashi, Y., Kremenetski, K., Paus, A., Pisaric, M. F. J., and Vokova, V. S.: Climate change and Arctic ecosys-
831 tems I. Vegetation changes north of 55°N between the last glacial maximum, mid-Holocene and present. *Journal of*
832 *Geophysical Research - Atmospheres*, 108(D19), doi: 10.1029/2002JD002558, 2003.
- 833 Bird, B. W., Abbott M. B., Rodbell D. T., and Vuille M.: Holocene tropical South American hydroclimate re-
834 vealed from a decadal resolved lake sediment $\delta^{18}O$ record, *Earth Planet. Sc. Lett.*, 310, 192-202,
835 doi:10.1016/j.epsl.2011.08.040, 2011.
- 836 Bobst, A. L., Lowenstein, T. K., Jordan, T. E., Godfrey, L. V., Ku, T.-L., and Luo, S.: A 106 ka paleoclimate
837 record from drill core of the Salar de Atacama, northern Chile, *Palaeogeogr. Palaeocl.*, 173, 21-42,
838 doi:10.1016/S0031-0182(01)00308, 2001.
- 839 Braconnot, P., Otto-Bleisner, B., Harrison, S.P., Joussaume, S., Peterschmitt, J.-Y., Abe-Ouchi, A., Crucifix, M.,
840 Driesschaert, E., Fichefet, T., Hewitt, C.D., Kagayama, M., Kitoh, A., Loutre, M.-F., Marti, O., Merkel, U.,
841 Ramstein, G., Valdes, P., Weber, L., Yu, Y., and Zhao, Y.: Results of PMIP2 coupled simulations of the mid-
842 Holocene and Last Glacial maximum, part 1: experiments and large-scale features, *Clim Past* 3:261–277, 2007.
- 844 Böhner, J.: General climatic controls and topoclimatic variations in Central and High Asia, *Boreas*, 35(2), 279-295,
845 2006.
- 846 Bookhagen, B., Thiede, R.C., and Strecker, M.R.: Late Quaternary intensified monsoon phases control landscape
847 evolution in the northwest Himalaya, *Geology*, 33(2), 149-152. doi: 10.1130/G20982.1, 2005.
- 848 Boos, W. R., and Kuang, Z.: Dominant control of the South Asian monsoon by orographic insulation versus plateau
849 heating, *Nature*, 463, 218-222, 2010.
- 850 Braun, J.: A simple model for regolith formation by chemical weathering: Regolith Formation, *Journal of Geophysical*
851 *Research Earth's Surface*, DOI: 10.1002/2016JF003914, 2016.
- 852 Caves, J.: Late Miocene Uplift of the Tian Shan and Altai and Reorganization of Central Asia Climate, *GSA*
853 *Today*, doi:10.1130/gsatg305a.1, 2017.

- 854 CLIMAP Project Members: Seasonal Reconstruction of the Earth's Surface at the Last Glacial Maximum.
855 *Map and Chart Series*, Vol. 36, Geological Society of America, 18 pp., 1981.
856
- 857 Cohen, S.J.: Bringing the global warming issue close to home: The challenge of regional impact studies. *Bulletin of the*
858 *American Meteorological Society*, 71: 520 – 526., 1990.
- 859 D'Agostino, K., Seltzer, G., Baker, P., Fritz, S., and Dunbar, R.: Late-Quaternary lowstands of Lake Titicaca:
860 evidence from high-resolution seismic data, *Palaeogeogr. Palaeoclimatol.*, 179, 97-111, doi:10.1016/S0031-
861 0182(01)00411-4, 2002.
- 862 De Batist, M., Fagel N., Loutre M. F., and Chapron E.: A 17,900-year multi-proxy lacustrine record of Lago
863 Puyehue (Chilean Lake District): introduction, *J. Paleolimnol.*, 39, 151-161, doi:10.1007/s10933-007-
864 9113-2, 2007.
- 865 de Porras, M. E., Maldonado, A., Abarzua, A. M., Cardenas, M. L., Francois, J. P., Martel-Cea, A., Stern, C.
866 R., Mendez, C., and Reyes, O.: Postglacial vegetation, fire and climate dynamics at Central Chilean
867 Patagonia (Lake Shaman, 44°S), *Quaternary Sci. Rev.*, 50, 71-85, doi:10.1016/j.quascirev.2012.06.015;
868 2012.
- 869 de Porras, M. E., Maldonado, A., Quintana, F. A., Martel-Cea, A., Reyes, O., and Méndez, C.: Environmental
870 and climatic changes in central Chilean Patagonia since the Late Glacial (Mallín El Embudo, 44° S), *Clim.*
871 *Past*, 10, 1063–1078, doi:10.5194/cp-10-1063-2014, 2014.
- 872 Delunel, R., van der Beek, P. A., Carcaillet, J., Bourlès, D. L., and Valla, P.G.: Frost-cracking control on catchment de-
873 nudation rates: Insights from in situ produced ¹⁰Be concentrations in stream sediments (Ecrins–Pelvoux massif,
874 French Western Alps), *Earth and Planetary Science Letters*, 293(1–2), 72–83, doi:10.1016/j.epsl.2010.02.020,
875 2010.
- 876 DeMenocal, P., Ortiz, J., Guilderson, T., Adkins, J., Samthein, M., Baker, L., and Yarusinsky, M.: Abrupt on-
877 set and termination of the African Humid Period:: rapid climate responses to gradual insolation forcing,
878 *Quaternary Sci. Rev.*, 19, 347-361, doi:10.1016/S0277-3791(99)00081-5, 2000.
- 879 Demske, D., Tarasov, P. E., Wünnemann, B., and Riedel, F.: Late glacial and Holocene vegetation, Indian
880 monsoon and westerly circulation in the Trans-Himalaya recorded in the lacustrine pollen sequence from
881 Tso Kar, Ladakh, NW India, *Palaeogeogr. Palaeoclimatol.*, 279, 172-185, doi:10.1016/j.palaeo.2009.05.008,
882 2009.
- 883 Diaz, F.P., Latorre, C., Maldonado, A., Quade, J., and Betancourt, J.L.: Rodent middens reveal episodic,
884 long-distance plant colonizations across the hyperarid Atacama Desert over the last 34,000 years, *J.*
885 *Biogeogr.*, 39, 510-525, doi:10.1111/j.1365-2699.2011.02617.x, 2012.
- 886 Dietrich, W. E., and Perron, J.T.: The search for a topographic signature of life, *Nature*, 439(7075), 411–418,
887 doi:10.1038/nature04452, 2006.
- 888 Dietrich, S., Werner, M., Spanghel, T., and Lohmann, G.: Influence of orbital forcing and solar activity on water iso-
889 topes in precipitation during the mid and late Holocene, *Clim. Past*, 9, 13-26. doi:10.5194/cp-9-13-2013, 2013.
890

- 891 Dettman, D.L., Fang, X.M., Garziona, C.N., and Li, J.J.: Uplift-driven climate change at 12 Ma: a long delta O-18 re-
892 cord from the NE margin of the Tibetan plateau. *Earth and Planetary Science Letters*, 214(1-2), 267-277, 2003.
- 893 Dowsett, H.J., Robinson, M., Haywood, A., Salzmann, U., Hill, D., Sohl, L., Chandler, M., Williams, M., Foley, K.,
894 and Stoll, D.: The PRISM3D paleoenvironmental reconstruction. *Stratigraphy*, 7, 123–139, 2010.
- 895 Egholm, D.L., Nielsen, S.B., Pedersen, V.K., Lesemann, J.,: Glacial effects limiting mountain height, *Nature*, 460(7257),
896 884-887, 2009.
- 897 Ehlers, T.A., and Poulsen, C.J.: Influence of Andean uplift on climate and paleoaltimetry estimates, *Earth and Planet-
898 ary Science Letters*, 281(3-4), 238-248, 2009.
- 899 Etheridge, D.M., Steele, L., Langenfelds, R., Francey, R., Barnola, J., and Morgan, V.,: Natural and anthropogenic
900 changes in atmospheric CO₂ over the last 1000 years from air in Antarctic ice and firn, *J Geophys Res* 101:4115–
901 4128, 1996.
- 902
- 903 Etheridge, D.M., L. Steele, R. Francey, and R. Langenfelds (1998), Atmospheric methane between 1000 a.d. and
904 present: evidence of anthropogenic emissions and climatic variability. *J Geophys Res*, 103:15979–15993
905
- 906 Feng, R., Poulsen, C.J., Werner, M., Chamberlain, C.P., Mix, H.T., and Mulch, A.: Early Cenozoic evolution of topo-
907 graphy, climate, and stable isotopes in precipitation in the North American Cordillera, *American Journal of Science*,
908 313(7), 613–648, 2013.
- 909 Feng, R., Poulsen, C.J., Werner, M., 2016. Tropical circulation intensification and tectonic extension recorded
910 by Neogene terrestrial d18O records of the western United States. *Geology* 44. doi:10.1130/G38212.1
911
- 912 Feng, R., Poulsen, C.J., 2016. Refinement of Eocene lapse rates, fossil-leaf altimetry, and North American
913 Cordilleran surface elevation estimates. *Earth Planet. Sci. Lett.* doi:10.1016/j.epsl.2015.12.022
914
- 915 Fritz, S. C., Baker, P. A., Lowenstein, T. K., Seltzer, G. O., Rigsby, C. A., Dwyer, G. S., Tapia, P. M., Arnold,
916 K. K., Ku, T. L., and Luo, S.: Hydrologic variation during the last 170,000 years in the southern hemisphere
917 tropics of South America, *Quaternary Res.*, 61, 95 – 104, doi:10.1016/j.yqres.2003.08.007, 2004. Gasse, F.,
918 Arnold, M., Fontes, J. C., Fort, M., Gibert, E., Huc, A., Li, B., Li, Y., Liu, Q., Melleres, F., Van Campo, E.,
919 Wang, F., and Zhang, Q.: A 13,000-year climate record from western Tibet, *Nature*, 353, 742-745,
920 doi:10.1016/j.quaint.2006.02.001, 1991.
- 921 Gayo E. M., Latorre, C., Santoro, C. M., Maldonado, A., and De Pol-Holz, R.: Hydroclimate variability in the
922 low-elevation Atacama Desert over the last 2500 yr, *Clim. Past*, 8, 287-306, doi:10.5194/cp-8-287-2012,
923 2012. Gierz, P., Lohmann, G., and Wei, W.: Response of Atlantic Overturning to future warming in a coupled at-
924 mosphere-ocean-ice sheet model, *Geophysical Research Letters*, 42, 6811-6818, doi:10.1002/2015GL065276,
925 2015.
- 926 Gilli, A., Ariztegui, D., Bradbury, J. P., Kelts, K. R., Markgraf, V., and McKenzie, J. A.: Tracking abrupt cli-
927 mate change in the Southern Hemisphere: a seismic stratigraphic study of Lago Cardiel, Argentina
928 (49°S), *Terra Nova*, 13, 443-448, doi:10.1046/j.1365-3121.2001.00377.x , 2001.
- 929 Glotzbach, C., van der Beek, P., Carcaillet, J., and Delunel, R.: Deciphering the driving forces of erosion rates on mil-
930 lennial to million-year timescales in glacially impacted landscapes: An example from the Western Alps, *Journal of*

- 931 *Geophysical Research: Earth Surface*, 118, 1491-1515, 2013.
- 932 Gong, X., Knorr, G., Lohmann, G., and Zhang, X.: Dependence of abrupt Atlantic meridional ocean circulation changes
933 on climate background states, *Geophysical Research Letters*, 40 (14), 3698-3704, doi:10.1002/grl.50701, 2013.
- 934 Grosjean, M., Van Leeuwen, J., Van der Knaap, W., Geyh, M., Ammann, B., Tanner, W., Messerli, B.,
935 Núñez, L., Valero-Garcés, B., and Veit, H. : A 22,000 14C year BP sediment and pollen record of climate
936 change from Laguna Miscanti (23°S), northern Chile, *Global Planet. Change*, 28, 35–51, doi:10.1016/
937 S0921-8181(00)00063-1, 2001.
- 938 Gyssels, G., Poesen, J., Bochet, E., and Li, Y.: Impact of plant roots on the resistance of soils to erosion by water: a re-
939 view, *Progress in Physical Geography*, 29, 189–217. <http://doi.org/10.1191/0309133305pp443ra>, 2005.
- 940 Hansen, B. C. S., Seltzer, G. O., and Wright Jr., H.E.: Late Quaternary vegetational change in the central
941 Peruvian Andes, *Palaeogeogr. Palaeoclimatol.*, 109, 263-285, doi:10.1016/0031-0182(94)90179-1, 1994.
- 942 Harris, I., Jones, P.D., Osborn, T.J., and Lister, D.H.: Updated high-resolution grids of monthly climatic observations -
943 the CRU TS3.10 Dataset, *International Journal of Climatology*, doi:10.1002/joc.3711, 2013.
- 944 Harrison, S. P., Yu, G., Takahara, H., and Prentice, I. C.: Palaeovegetation - Diversity of temperate plants in east Asia.
945 *Nature* 413, 129-130, 2001.
946
- 947 Harrison, S.P., Bartlein, P.J., Brewer, S., Prentice, I.C., Boyd, M., Hessler, I., Holmgren, K., Izumi, K., and Willis, K.:
948 Climate model benchmarking with glacial and mid-Holocene climates, *Climate Dynamics*, 43, 671-688. doi
949 10.1007/s00382-013-1922-6, 2013.
- 950 Haywood, A.M., Valdes, P.J., and Sellwood, B.W.: Global scale palaeoclimate reconstruction of the middle Pliocene
951 climate using the UKMO GCM: initial results. *Global and Planetary Change*, 25 (3–4), 239–256, 2000.
- 952 Haywood, A.M., Dowsett, H.J., Otto-Bliesner, B., Chandler, M.A., Dolan, A.M., Hill, D.J., Lunt, D.J., Robinson, M.M.,
953 Rosenbloom, N., Salzmann, U., and Sohl, L.E.: Pliocene Model Intercomparison Project (PlioMIP): experimental
954 design and boundary conditions (Experiment 1), *Geoscientific Model Development* (3), 227-242, 2010.
955
- 956 Haywood, A.M., Hill, D.J., Dolan, A.M., Otto-Bliesner, B., Bragg, F., Chan, W.-L., Chandler, M.A., Contoux, C., Jost,
957 A., Kamae, Y., Lohmann, G., Lunt, D.J., Abe-Ouchi, A., Pickering, S.J., Ramstein, G., Rosenbloom, N.A., Sohl, L.,
958 Stepanek, C., Yan, Q., Ueda, H., and Zhang, Z.: Large-scale features of Pliocene climate: results from the Pliocene
959 Model Intercomparison Project, *Clim. Past*, 9, 191-209. doi:10.5194/cp-9-191-2013, 2013.
960
- 961 Herman, F., Seward, D., Valla, P.G., Carter, A., Kohn, B., Willett, S.D., and Ehlers, T.A.: Worldwide acceleration of
962 mountain erosion under a cooling climate, *Nature*, 504, 423–426. doi:10.1038/nature12877, 2013.
- 963 Herzsuh, U., Kuerschner, H., and Mischke, S.: Temperature variability and vertical vegetation belt shifts
964 during the last ~50,000 yr in the Qilian Mountains (NE margin of the Tibetan Plateau, China), *Quaternary*
965 *Res.*, 66, 133-146, doi:10.1016/j.yqres.2006.03.001, 2006a.

- 966 Herzs Schuh, U., Winter, K., Wuennemann, B., and Li, S.: A general cooling trend on the central Tibetan
967 Plateau throughout the Holocene recorded by the lake Zigetang pollen spectra, *Quatern. Int.*, 154, 113-
968 121, doi:10.1016/j.quaint.2006.02.005, 2006b.
- 969
970 Herzs Schuh, U., Kramer A., Mischke S., and Zhang C.: Quantitative climate and vegetation trends since the
971 late glacial on the northeastern Tibetan Plateau deduced from Koucha lake pollen spectra, *Quaternary*
972 *Res.*, 71, 162-171, doi:10.1016/j.yqres.2008.09.003, 2009.
- 973 Hillenbrand, C.-D., and Fütterer, D.K.: Neogene to Quaternary deposition of opal on the continental rise west of the
974 Antarctic Peninsula, ODP Leg 178, Sites 1095, 1096, and 1101. In: Barker, P.F., Camerlenghi, A., Acton, G.D.,
975 Ramsay, A.T.S. (Eds.), *Proceedings of the Ocean Drilling Programme, Scientific Results*, 178. Texas A and M Uni-
976 versity, College Station, Texas, pp. 1–40 (CD-ROM), 2002.
- 977 Hillyer, R., Valencia, B. G., Bush, M.B., Silman, M.R., and Steinitz-Kannan, M.: A 24,700-yr paleolimnological
978 history from the Peruvian Andes, *Quaternary Res.*, 71, 71-82, doi:10.1016/j.yqres.2008.06.006, 2009.
- 979 Hobley, D.E., Sinclair, H.D., and Cowie, P.A.: Processes, rates, and time scales of fluvial response in an ancient post-
980 glacial landscape of the northwest Indian Himalaya. *Geological Society of America Bulletin*, 122, 1569-1584, 2010.
- 981 Hodell, D. A., Brenner, M., Kanfoush, S. L., Curtis, J. H., Stoner, J. S., Song, X., Wu, Y., and Whitmore, T. J.:
982 Paleoclimate of southwestern China for the past 50,000 yr inferred from lake sediment records, *Quatern-*
983 *ary Res.*, 52, 369-380, doi:10.1006/qres.1999.2072, 1999.
- 984 Hu, G., Yi, C.-L., Zhang, J.-F., Liu, J.-L., Jiang, T., and Qin, X.: Optically stimulated luminescence dating of a
985 moraine and a terrace in Laohugou valley, western Qilian Shan, northeastern Tibet, *Quaternary Interna-*
986 *tional* 321, 37-49, doi:10.1016/j.quaint.2013.12.019, 2014.
- 987 Insel, N., Poulsen, C.J., and Ehlers, T.A.: Influence of the Andes Mountains on South American moisture transport,
988 convection, and precipitation, *Climate Dynamics*, 35 (7-8), 1477-1492, 2010.
- 989 Jeffery, M.L., Ehlers, T.A., Yanites, B.J., and Poulsen, C.J.: Quantifying the role of paleoclimate and Andean Plateau
990 uplift on river incision: PALEOCLIMATE ROLE IN RIVER INCISION, *Journal of Geophysical Research: Earth*
991 *Surface*, 118(2), 852–871, doi:10.1002/jgrf.20055, 2013.
- 992 Jenny, B., Valero-Garces, B. L., Urrutia, R., Kelts, K., Veit, H., and Geyh, M.: Moisture changes and
993 fluctuations of the Westerlies in Mediterranean Central Chile during the last 2000 years: The Laguna
994 Aculeo record (33°50' S), *Quatern. Int.*, 87, 3-18, doi:10.1016/S1040-6182(01)00058-1, 2002a.
- 995 Jenny, B., Valero-Garcés, B.L., Villa-Martínez, R., Urrutia, R., Geyh, M. A., and Veit, H.: Early to Mid-Holo-
996 cene Aridity in Central Chile and the Southern Westerlies: The Laguna Aculeo Record (34°S), *Quaternary*
997 *Res.*, 58, 160–170, doi:10.1006/qres.2002.2370, 2002b.
- 998 Jungclaus, J. H., Lorenz, S. J., Timmreck, C., Reick, C. H., Brovkin, V., Six, K., Segschneider, J., Giorgetta, M.A.,
999 Crowley, T.J., Pongratz, J., Krivova, N.A., Vieira, L.E., Solanski, S.K., Klocke, D., Botzet, M., Esch, M., Gayler,
1000 V., Haak, H., Raddatz, T.J., Roeckner, E., Schnur, R., Widmann, H., Claussen, M., Stevens, B., and Marotzke, J.:
1001 Climate and carbon-cycle variability over the last millennium. *Climate of the Past*, 6, 723-737. doi:10.5194/cp-6-723-
1002 2010, 2010.

- 1003 Junginger, A., Roller, S., Olaka, L. A., and Trauth, M. H.: The effects of solar irradiation changes on the mi-
1004 gration of the Congo Air Boundary and water levels of paleo-Lake Suguta, Northern Kenya Rift, during the
1005 African Humid Period (15–5 ka BP), *Palaeogeogr. Palaeoclimatol.*, 396, 1–16, doi:10.1016/
1006 j.palaeo.2013.12.007, 2014.
- 1007 Kaiser, J., Schefuss, E., Lamy, F., Mohtadi, M., and Hebbeln, D.: Glacial to Holocene changes in sea surface
1008 temperature and coastal vegetation in north central Chile : high versus low latitude forcing, *Quaternary*
1009 *Sci. Rev.*, 27, 2064–2075, doi:10.1016/j.quascirev.2008.08.025, 2008.
- 1010 Kalnay, E., Kanamitsu, M., Kistler, R., Collins, W., Deaven, D., Gandin, L., Iredell, M., Saha, S., White, G., Woollen,
1011 J., Zhu, Y., Chelliah, M., Ebisuzaki, W., Higgins, W., Janowiak, J., Mo, K.C., Ropelewski, C., Wang, J., Leetmaa,
1012 A., Reynolds, R., Jenne, R., and Joseph, D.: The NCEP/NCAR 40-year reanalysis project. *Bulletin of the American*
1013 *Meteorological Society*, 77(3), 437–471, 1996.
- 1014 Kashiwaya, K., Masuzawa, T., Morinaga, H., Yaskawa, K., Yuan, B. Y., Liu, J. Q., and Gu, Z.: Changes in
1015 hydrological conditions in the central Qing-Zang (Tibetan) Plateau inferred from lake bottom sediments,
1016 *Earth Planet. Sc. Lett.*, 135, 31–39, doi:10.1016/0012-821X(95)00136-Z, 1995.
- 1017 Kent-Corson, M., Sherman, L., Mulch, A. and Chamberlain, C.: Cenozoic topographic and climatic response
1018 to changing tectonic boundary conditions in Western North America, *Earth Planet. Sc. Lett.*, 252(3–4),
1019 453–466, doi:10.1016/j.epsl.2006.09.049, 2006.
- 1020 Kistler, R., Collins, W., Saha, S., White, G., Woollen, J., Kalnay, E., Chelliah, M., Ebisuzaki, W., Kanamitsu, M.,
1021 Kousky, V., Van den Dool, H., Jenne, R., and Fiorino, M.: The NCEP–NCAR 50–Year Reanalysis: Monthly Means
1022 CD–ROM and Documentation. *Bulletin of the American Meteorological Society*, 82(2), 247–267, 2001.
- 1023 Kirchner, J.W., Finkel, R.C., Riebe, C.S., Granger, D.E., Clayton, J.L., King, J.G., and Megahan, W.F.: Mountain
1024 erosion over 10 yr, 10 k.y., and 10 m.y. time scales, *Geology*, 29 (7), 591–594, 2001.
- 1025 Knorr, G., Butzin, M., Micheels, A., and Lohmann, G.: A Warm Miocene Climate at Low Atmospheric CO₂ levels.
1026 *Geophysical Research Letters*, 38, L20701, doi:10.1029/2011GL048873, 2011.
- 1027 Koons, P.O., Zeitler, P.K., and Hallet, B.: 5.14 Tectonic Aneurysms and Mountain Building, in *Treatise on Geomor-*
1028 *phology*, pp. 318–349, Elsevier, 2013.
- 1029 Kotlia, B. S., Sharma, C., Bhalla, M. S., Rajagopalan, G., Subrahmanyam, K., Bhattacharya, A., and
1030 Valdiya, K. S.: Paleoclimatic conditions in the late Pleistocene Wadda Lake, eastern Kumaun Himalaya
1031 (India), *Palaeogeogr. Palaeoclimatol.*, 162, 105–118, doi:10.1016/S0031-0182(00)00107-3, 2000.
- 1032 Kramer, A., Herzschuh, U., Mischke, S., and Zhang, C.: Late glacial vegetation and climate oscillations on
1033 the southeastern Tibetan Plateau inferred from the lake Naleng pollen profile, *Quaternary Res.*, 73, 324–
1034 335, doi:10.1016/j.yqres.2009.12.003, 2010.
- 1035 Kraus, H.: *Die Atmosphäre der Erde. Eine Einführung in die Meteorologie.* Berlin, 2001.
- 1036 Kutzbach, J.E., Guetter, P.J., Ruddiman, W.F., and Prell, W.L.: Sensitivity of Climate to Late Cenozoic Uplift in

- 1037 Southern Asia and the American West - Numerical Experiments, *Journal of Geophysical Research-Atmospheres*,
1038 94(D15), 18393-18407, 1989.
- 1039 Kutzbach, J.E., Prell, W.L., and Ruddiman, W.F.: Sensitivity of Eurasian Climate to Surface Uplift of the Tibetan Plat-
1040 eau, *Journal of Geology*, 101(2), 177-190, 1993.
- 1041 Lamy, F. and Kaiser, J.: Past Climate Variability in South America and Surrounding Regions, Chapter 6:
1042 Glacial to Holocene Paleoceanographic and Continental Paleoclimate Reconstructions Based on ODP
1043 Site 1233/GeoB 3313 Off southern Chile, 2009.
- 1044 Lamy, F., Hebbeln, D., and Wefer, G.: High Resolution Marine Record of Climatic Change in Mid-latitude
1045 Chile during the Last 28,000 Years Based on Terrigenous Sediment Parameters, *Quaternary Res.*, 51,
1046 83-93, doi:10.1006/qres.1998.2010, 1999.
- 1047 Lamy, F., Klump, J., Hebbeln, D., and Wefer, G.: Late Quaternary rapid climate change in northern Chile,
1048 *Terra Nova*, 12, 8-13, doi:10.1046/j.1365-3121.2000.00265.x, 2000.
- 1049 Lamy, F., Rühlemann, C., Hebbeln, D. and Wefer, G.: High- and low-latitude climate control on the position
1050 of the southern Peru-Chile Current during the Holocene, *Paleoceanography*, 17, 16-1-16-10,
1051 doi:10.1029/2001PA000727, 2002.
- 1052 Latorre, C., Betancourt, J., Rylander, K., and Quade, J.: Vegetation invasions into absolute desert: A 45 000
1053 yr rodent midden record from the Calama-Salar de Atacama basins, northern Chile (lat 22° - 24°S), *Geol.*
1054 *Soc. Am. Bull.*, 114, 349-366, doi:10.1130/0016-7606(2002)114<0349:VIIADA>2.0.CO;2, 2002.
- 1055 Latorre, C., Betancourt, J.L., Rylander, K.A., Quade, J., and Matthei, O.: A vegetation history from the arid
1056 prepuna of northern Chile (22-23°S) over the last 13500 years, *Palaeogeogr. Palaeoclimatol.*, 194, 223-246,
1057 doi:10.1016/S0031-0182(03)00279-7, 2003.
- 1058 Latorre, C., Betancourt, J.L., and Arroyo, M.T.K.: Late Quaternary vegetation and climate history of a peren-
1059 nial river canyon in the Río Salado basin (22°S) of northern Chile, *Quaternary Res.*, 65, 450-466,
1060 doi:10.1016/j.yqres.2006.02.002, 2006.
- 1061 Lechler, A. and Niemi, N.: Sedimentologic and isotopic constraints on the Paleogene paleogeography and
1062 paleotopography of the southern Sierra Nevada, California, *Geology*, 39(4), 379-382,
1063 doi:10.1130/g31535.1, 2011.
- 1064 Lechler, A., Niemi, N., Hren, M. and Lohmann, K.: Paleoelevation estimates for the northern and central
1065 proto-Basin and Range from carbonate clumped isotope thermometry, *Tectonics*, 32(3), 295-316,
1066 doi:10.1002/tect.20016, 2013.
- 1067 Lease, R.O., and Ehlers, T.A.: Incision into the Eastern Andean Plateau During Pliocene Cooling, *Science*, 341(6147),
1068 774-776, doi:10.1126/science.1239132, 2013.
- 1069 Legates, D.R., and Willmott, C.J.: Mean Seasonal and Spatial Variability in Gauge-Corrected, Global Precipitation, *In-*
1070 *ternational Journal of Climatology* 10(2), 111-127. doi: 10.1002/joc.3370100202, 1990.
- 1071 Li, J., Ehlers, T.A., Werner, M., Mutz, S.G., Steger, C., Paeth, H.: Late quaternary climate, precipitation $\delta^{18}\text{O}$, and In-
1072 dian monsoon variations over the Tibetan Plateau. *Earth and Planetary Science Letters* 457, 412-422, 2017.
- 1073 Liu, X., Colman, S. M., Brown, E. T., An, Z., Zhou, W., Jull, A. J. T., Huang, Cheng, Y., P., Liu, W., and Xu,
1074 H.: A climate threshold at the eastern edge of the Tibetan plateau, *Geophys. Res. Lett.*, doi:

- 1075 10.1002/2014GL060833, 2014.
- 1076 Licht, A., Quade, J., Kowler, A., de los Santos, M., Hudson, A., Schauer, A., Huntington, K., Copeland, P.
1077 and Lawton, T.: Impact of the North American monsoon on isotope paleoaltimeters: Implications for the
1078 paleoaltimetry of the American southwest, *Am. J. Scie*, 317(1), 1-33, doi:10.2475/01.2017.01, 2017.
- 1079 Lohmann, G., Pfeiffer, M., Laepple, T., Leduc, G., and Kim, J.-H.: A model-data comparison of the Holocene global
1080 sea surface temperature evolution. *Clim. Past*, 9, 1807-1839, doi:10.5194/cp-9-1807-2013, 2013.
1081
- 1082 Lorenz, S.J., and Lohmann, G.: Acceleration technique for Milankovitch type forcing in a coupled atmosphere-ocean
1083 circulation model: method and application for the Holocene. *Climate Dynamics* (2004) 23: 727. doi:10.1007/
1084 s00382-004-0469-y, 2004.
1085
- 1086 Maldonado, A. and Villagrán, C.: Climate variability over the last 9900 cal yr BP from a swamp forest pollen
1087 record along the semiardi coast of Chile, *Quaternary Res.*, 66, 146-258, doi:10.1016/j.yqres.2006.04.003,
1088 2006.
- 1089 Maldonado, A. J., Betancourt, J. L., Latorre, C., and Villagrán, C : Pollen analyses from a 50000-yr rodent
1090 midden series in the southern Atacama Desert (25°30' S), *J. Quaternary Sci.*, 20, 493-507,
1091 doi:10.1002/jqs.936, 2005.
- 1092 Maldonado, A., Méndez, C., Ugalde, P., Jackson, D., Seguel, R., and Latorre, C.: Early Holocene climate
1093 change and human occupation along the semiarid coast of north-central Chile, *J. Quaternary Sci.*, 25,
1094 985–988, doi:10.1002/jqs.1385, 2010.
- 1095 Markgraf, V., Bradbury, J. P., Schwab, A., Burns, S., Stern, C., Ariztegui, D., Gilli, D., Anselmetti, F. S.,
1096 Stine, S., and Maidana, N.: Holocene palaeoclimates of southern Patagonia: limnological and
1097 environmental history of Lago Cardiel, Argentina, *Holocene*, 13, 581–591,
1098 doi:10.1191/0959683603hl648rp, 2003.
- 1099 Markgraf, V., Whitlock, C., and Haberle, S.: Vegetation and fire history during the last 18,000 cal yr B.P. in
1100 Southern Patagonia: Mallín Pollux, Coyhaique, Province Aisén (45°41'30" S, 71°50'30" W, 640 m
1101 elevation), *Palaeogeogr. Palaeocl*, 254, 492–507, doi:10.1016/j.palaeo.2007.07.008, 2007.
- 1102 Maroon, E. A., Frierson, D. M. W., and Battisti, D. S.: The tropical precipitation response to Andes
1103 topography and ocean heat fluxes in an aquaplanet model, *J. Climate*, 28, 381–398, doi:10.1175/JCLI-D-
1104 14-00188.1, 2015.
- 1105 Maroon, E. A., Frierson, D. M. W., Kang, S. M., and Scheff, J.: The precipitation response to an idealized
1106 subtropical continent, *J. Climate*, 29, 4543–4564, doi:10.1175/JCLI-D-15-0616.1, 2016.
- 1107 Marshall, J.A., Roering, J.J., Bartlein, P.J., Gavin, D.G., Granger, D.E., Rempel, A.W., Praskievicz, S.J., and Hales,
1108 T.C.: Frost for the trees: Did climate increase erosion in unglaciated landscapes during the late Pleistocene? *Science*
1109 *Advances*, 1, 1-10, 2015.
- 1110 Marston, R.A.: Geomorphology and vegetation on hillslopes: Interactions, dependencies, and feedback loops, *Geomor-*
1111 *phology*, 116(3–4), 206–217. doi:http://doi.org/10.1016/j.geomorph.2009.09.028, 2010.
- 1112 Matsuoka, N., and Murton, J.: Frost weathering: Recent advances and future directions. *Permafr. Periglac. Process.* 19,
1113 195–210, 2008.
- 1114 Matsuoka, N.: Solifluction rates, processes and landforms: A global review. *Earth Science Reviews* 55, 107–134, 2001.

- 1115 Maussion, F., Scherer, D., Mölg, T., Collier, E., Curio, J., and Finkelnburg, R.: Precipitation seasonality and variability
1116 over the Tibetan Plateau as resolved by the High Asia Reanalysis, *J. Climate*, 27, 1910-1927, doi:10.1175/JCLI-D-
1117 13-00282.1, 2014
- 1118 Méndez, C., Gil, A., Neme, G., Nuevo Delaunay, A., Cortegoso, V., Huidobro, C., Durán, and Maldano, A.:
1119 Mid Holocene radiocarbon ages in the Subtropical Andes (~29° - 35° S), climatic change an implicaton for
1120 human space organization, *Quatern. Int.*, 356, 15-26, doi:10.1016/j.quaint.2014.06.059, 2015.
- 1121 Mesinger, F., DiMego, G., Kalnay, E., Mitchell, K., Shafran, P.C., Ebisuzaki, W., Jovic, D., Woollen, J., Rogers, E.,
1122 Berbery, E.H., Ek, M.B., Fan, Y., Grumbine, R., Higgins, W., Li, H., Lin, Y., Manikin, G., Parrish, D., and Shi,
1123 W.:North American Regional Reanalysis, *Bulletin of the American Meteorological Society*, 87, 343–
1124 360.doi:10.1175/BAMS-87-3-343, 2006.
- 1125 Methner, K., Fiebig, J., Wacker, U., Umhoefer, P., Chamberlain, C. and Mulch, A.: Eocene-Oligocene proto-
1126 Cascades topography revealed by clumped ($\Delta 47$) and oxygen isotope ($\delta 18O$) geochemistry (Chumstick
1127 Basin, WA, USA), *Tectonics*, 35(3), 546-564, doi:10.1002/2015tc003984, 2016.
- 1128 Mischke S., Kramer M., Herzs Schuh U., Shang H., Erzinger J., and Zhang C.: Reduced early holocene
1129 moisture availability in the Bayan Har Mountains, northeastern Tibetan Plateau, inferred from a multi-
1130 proxy lake record, *Palaeogeogr. Palaeoclimatol.*, 267, 59-76, doi:10.1016/j.palaeo.2008.06.002, 2008.
- 1131 Molnar, P., Boos, W.R., and Battisti, D.S.: Orographic Controls on Climate and Paleoclimate of Asia: Thermal and
1132 Mechanical Roles for the Tibetan Plateau, *Annual Review of Earth and Planetary Sciences*, 38, 77-102, 2010.
- 1133 Molnar, P., and England, P.: Late Cenozoic uplift of mountain ranges and global climate change: chicken or egg?,
1134 *Nature*, 346, 29-34, 1990.
- 1135 Montgomery, D.R.: Slope distributions, threshold hillslopes, and steady-state topography, *American Journal of Science*,
1136 301, 432-454, 2001.
- 1137 Montgomery, D.R., Balco, G., and Willett, S.D.: Climate, tectonics, and the morphology of the Andes, *Geology*, 29(7),
1138 579-582, 2001.
- 1139 Moon, S., Chamberlain, C.P., Blisniuk, K., Levine, N., Rood, D.H., Hilley, G.E.: Climatic control of denudation in the
1140 deglaciaded landscape of the Washington Cascades, *Nature Geoscience*, 4, 469-473, 2011.
- 1141 Moreno, A., Santoro, C. M., and Latorre, C.: Climate change and human occupation in the northernmost
1142 Chilean Altiplano over the last ca. 11500 cal. a BP, *Quaternary Sci.*, 24, 373–382, doi:10.1002/jqs.1240,
1143 2009.
- 1144 Morinaga, H., Itota, C., Isezaki, N., Goto, H., Yaskawa, K., Kusakabe, M., Liu, J., Gu, Z., Yuan, B., and Cong,
1145 S.: Oxygen-18 and carbon-13 records for the last 14,000 years from lacustrine carbonates of Siling-Co
1146 (lake) in the Qinghai-Tibetan Plateau, *Geophys. Res. Lett.*, 20, 2909-2912, doi:10.1029/93GL02982,
1147 1993.
- 1148 Morrill, C., Overpeck, J. T., Cole, J. E., Liu, K., Shen, C., and Tang, L.: Holocene variations in the Asian mon-
1149 soon inferred from the geochemistry of lake sediments in central Tibet, *Quaternary Res.*, 65, 232-243,
1150 doi:10.1016/j.yqres.2005.02.014, 2006.

- 1151 Moulton, K.L., and Berner, R.A.: Quantification of the effect of plants on weathering: studies in Iceland, *Geology*, 26,
1152 895-898, 1998.
- 1153 Muegler, I., Gleixner, G., Guenther, F., Maeusbacher, R., Daut, G., Schuett, B., Berking, J., Schwalb, A.,
1154 Schwark, L., Xu, B., Yao, T., Zhu, L., and Yi, C.: A multi-proxy approach to reconstruct hydrological
1155 changes and Holocene climate development of Nam Co, Central Tibet, *J. Paleolimnol.*, 43, 625-648,
1156 doi:10.1007/s10933-009-9357-0, 2010.
- 1157 Mujica, M. I., Latorre, C., Maldonado, A., González-Silvestre, L., Pinto, R., De Pol-Holz, R., and Santoro, C.
1158 M.: Late Quaternary climate change, relict populations and present-day refugia in the northern Atacama
1159 Desert: a case study from Quebrada La Higuera (18° S), *J. Biogeogr.*, 42, 76–88, doi:10.1111/jbi.12383,
1160 2015.
- 1161 Mulch, A., Sarna-Wojcicki, A., Perkins, M. and Chamberlain, C.: A Miocene to Pleistocene climate and
1162 elevation record of the Sierra Nevada (California), *P. Natl. Acad. Sci. USA*, 105(19), 6819-6824,
1163 doi:10.1073/pnas.0708811105, 2008.
- 1164
1165 Mulch, A., Chamberlain, C., Cosca, M., Teyssier, C., Methner, K., Hren, M. and Graham, S.: Rapid change in
1166 high-elevation precipitation patterns of western North America during the Middle Eocene Climatic Op-
1167 timum (MECO), *Am. J. Scie.*, 315(4), 317-336, doi:10.2475/04.2015.02, 2015.
- 1168 Mutz, S.G., Ehlers, T.A., Li, J., Steger, C., Peath, H., Werner, M., Poulsen, C.J.: Precipitation $\delta^{18}\text{O}$ over the South Asia
1169 Orogen from ECHAM5-wiso Simulation: Statistical Analysis of Temperature, Topography and Precipitation.
1170 *Journal of Geophysical Research-Atmospheres*, 121(16),9278-9300, doi: 10.1002/2016JD024856, 2016.
- 1171 Nishimura, M., Matsunaka, T., Morita, Y., Watanabe, T., Nakamura, T., Zhu, L., Nara, W. F., Imai, A., Izutsu,
1172 Y., and Hasuike, N.: Paleoclimatic changes on the southern Tibetan Plateau over the past 19,000 years
1173 recorded in lake Pumoyum Co, and their implications for the southwest monsoon evolution, *Palaeogeogr.*
1174 *Palaeocl.*, 396, 75-92, doi:10.1016/j.palaeo.2013.12.015, 2014.
- 1175 Otto-Bliesner, B.L., Brady, C.B., Clauzet, G., Tomas, R., Levis, S., and Kothavala, Z.: Last Glacial Maximum and
1176 Holocene Climate in CCSM3. *Journal of Climate*, 19, 2526-2544, 2006.
- 1177 Paeth, H.: Key Factors in African Climate Change Evaluated by a Regional Climate Model, *Erdkunde*, 58, 290-315,
1178 2004.
- 1179 Peel, M.C., Finlayson, B.L., McMahon, T.A.: Updated world map of the Koppen- Geiger climate classification.
1180 *Hydrol. Earth Syst. Sci.* 11, 1633–1644, 2007.
- 1181
1182 Pfeiffer, M., and Lohmann, G.: Greenland Ice Sheet influence on Last Interglacial climate: global sensitivity studies
1183 performed with an atmosphere-ocean general circulation model. *Climate of the Past*, 12, pp. 1313-1338,
1184 doi:10.5194/cp-12-1313-2016, 2016.
- 1185 Pickett, E.J., Harrison, S.P., Flenley, J., Grindrod, J., Haberle, S., Hassell, C., Kenyon, C., MacPhail, M., Martin, H.,
1186 Martin, A.H., McKenzie, M., Newsome, J.C., Penny, D., Powell, J., Raine, J.I., Southern, W., Stevenson, J., Sutra,
1187 J.-P., Thomas, I., van der Kaars, S., Ward, J.: Pollen-based reconstructions of biome distributions for Australia,
1188 South-East Asia and the Pacific (SEAPAC region) at 0, 6000 and 18,000 14C years B.P.. *Journal of Biogeography*,
1189 31, 1381–1444, doi: 10.1111/j.1365-2699.2004.01001.x, 2004.
- 1190
1191 Pingel, H., Mulch, A., Alonso, R., Cottle, J., Hynek, S., Poletti, J., Rohrmann, A., Schmitt, A., Stockli, D. and

- 1192 Strecker, M.: Surface uplift and convective rainfall along the southern Central Andes (Angastaco Basin,
1193 NW Argentina), *Earth Planet. Sc. Lett.*, 440, 33-42, doi:10.1016/j.epsl.2016.02.009, 2016.
- 1194
- 1195 Prentice, I. C., Jolly, D., and BIOME 6000 Participants. (2000). Mid-Holocene and glacial-maximum vegetation geo-
1196 graphy of the northern continents and Africa. *Journal of Biogeography* 27, 507-519.
- 1197
- 1198 Pueyo, J. J., Sáez, A., Giralt, S., Valero-Garcés, B.L., Moreno, A., Bao, R., Schwalb, A., Herrera, C., Klo-
1199 sowska, B., and Taberner, C.: Carbonate and organic matter sedimentation and isotopic signatures in
1200 Lake Chungará, Chilean Altiplano, during the last 12.3 kyr, *Palaeogeogr. Palaeocl.*, 307, 339-355,
1201 doi:10.1016/j.palaeo.2011.05.036, 2011.
- 1202 Quade, J., Rech, J. A., Betancourt, J. L., Latorre, C., Quade, B., Rylander, K. A., and Fisher, T.: Paleowet-
1203 lands and regional climate change in the central Atacama Desert, northern Chile, *Quaternary Res.*, 69,
1204 343-360, doi:10.1016/j.yqres.2008.01.003, 2008.
- 1205 Raymo, M.E., and Ruddiman, W.F.: Tectonic forcing of late cenozoic climate. *Nature*, 359(6391), 117-122, 1992.
- 1206 Rech, J. A., Pigati, J. S., Quade, J., and Betancourt, J. L.: Re-evaluation of mid-Holocene deposits at
1207 Quebrada Puripica, northern Chile, *Palaeogeogr. Palaeocl.*, 194, 207-222, doi:0.1016/S0031-
1208 0182(03)00278-5, 2003.
- 1209 Robinson, M.M.: New quantitative evidence of extreme warmth in the Pliocene Arctic, *Stratigraphy* 6, 265–275, 2009.
- 1210 Roeckner, E., Bäuml, G., Bonaventura, L., Brokopf, R., Esch, M., Giorgetta, M., Hagemann, S., Kirchner, I., Korn-
1211 blueh, L., Manzini, E., Rhodin, A., Schlese, U., Schulzweida, U., and Tompkins, A.: The atmospheric general circu-
1212 lation model ECHAM5. Part I: Model description. Rep. 349Rep., 127 pp, Max Planck Institute for Meteorology,
1213 Hamburg, 2003.
- 1214 Roering, J.J., Marshall, J., Booth, A.M., Mort, M., and Jin, Q.: Evidence for biotic controls on topography and soil pro-
1215 duction, *Earth and Planetary Science Letters*, 298(1–2), 183–190, doi:10.1016/j.epsl.2010.07.040, 2010.
- 1216 Salzmann, U., Williams, M., Haywood, A.M., Johnson, A.L.A., Kender, S., and Zalasiewicz, J.: Climate and environ-
1217 ment of a Pliocene warm world. *Palaeogeography, Palaeoclimatology, Palaeoecology*, 309 (1-8), 2011.
- 1218 Sarnthein, M.: Sand deserts during glacial maximum and climatic optimum, *Nature*, 272, 43–46,
1219 doi:10.1038/272043a0, 1978.
- 1220 Sarnthein, M., Gersonde, R., Niebler, S., Pflaumann, U., Spielhagen, R., Thiede, J., Wefer, G., Weinelt, M.: Overview
1221 of Glacial Atlantic Ocean Mapping (GLAMAP 2000), *Paleoceanography*, 18(2), doi:10.1029/2002PA000769,
1222 2003.
- 1223 Schäfer-Neth C., and Paul, A.: The Atlantic Ocean at the last glacial maximum: objective mapping of the GLAMAP
1224 sea-surface conditions. In: Wefer G, Mulitza S, Ratmeyer V (eds) *The South Atlantic in the late quaternary: recon-
1225 struction of material budgets and current systems*. Springer, Berlin, pp 531–548, 2003.

- 1226 Schaller, M., von Blanckenburg, F., Veldkamp, A., Tebbens, L.A., Hovius, N., and Kubik, P.W.: A 30 000 yr record of
1227 erosion rates from cosmogenic ^{10}Be in Middle European river terraces, *Earth and Planetary Science Letters*,
1228 204(1), 307–320, 2002.
- 1229 Schaller, M., and Ehlers T.A.: Limits to quantifying climate driven changes in denudation rates with cosmogenic radio-
1230 nuclides, *Earth and Planetary Science Letters*, v. 248, pp. 153-167. doi:10.1016/j.epsl.2006.05.027, 2006.
- 1231 Schwalb, A., Burns, S., and Kelts, K.: Holocene environments from stable isotope stratigraphy of ostracods
1232 and authigenic carbonate in Chilean Altiplano Lakes, *Palaeogeogr. Palaeocl.*,148, 153-168, doi:10.1016/
1233 S0031-0182(98)00181-3, 1999.
- 1234 Shen J., Liu X. Q., Wang S. M., and Matsumoto R.: Palaeoclimatic changes in the Qinghai, Lake area during
1235 the last 18,000 years, *Quatern. Int.*, 136, 131-140, doi:10.1016/j.quaint.2004.11.014, 2005.
- 1236 Shen C., Liu K., Tang L., and Overpeck J. T.: Quantitative relationships between modern pollen rain and cli-
1237 mate in the Tibetan Plateau. *Rev. Palaeobot. Palyno.*, 140, 61–77, doi:10.1016/j.revpalbo.2006.03.001,
1238 2006.
- 1239 Siani, G., Colin, C., Michel, E., Carel, M., Richter, T., Kissel, C., and Dewilde, F.: Late Glacial to Holocene
1240 terrigenous sediment record in the Northern Patagonian margin: Paleoclimate implications, *Palaeogeogr.*
1241 *Palaeocl.*, 297, 26-36, doi:10.1016/j.palaeo.2010.07.011, 2010.
- 1242 Simmons, A.J., Burridge, D.M., Jarraud, M., Girard, C., and Wergen, W.: The ECMWF Medium-Range prediction
1243 models development of the numerical formulations and the impact of increased resolution, *Meteorology and Atmo-*
1244 *spheric Physics*, 40(1-3), 28-60, 1989.
- 1245 Sohl, L.E., Chandler, M.A., Schmunk, R.B., Mankoff, K., Jonas, J.A., Foley, K.M., and Dowsett, H.J.: PRISM3/GISS
1246 topographic reconstruction, *U.S. Geological Survey Data Series*, 419, 6p., 2009.
1247
- 1248 Sowers T., Alley, R.B., and Jubenville, J.: Ice core records of atmospheric N_2O covering the last 106,000 years. *Sci-*
1249 *ence*, 301:945–948, 2003.
1250
- 1251 Stepanek, C., and Lohmann, G.: Modelling mid-Pliocene climate with COSMOS , *Geosci. Model Dev.* , 5 , pp. 1221-
1252 1243 . doi:10.5194/gmd-5-1221-2012, 2012.
- 1253 Stine, S. and Stine M.: A record from Lake Cardiel of climate change in southern South America, *Nature*,
1254 345, 705-708, doi:10.1038/345705a0,1990.
- 1255 Szeicz, J. M., Haberle, S. G., and Bennett, K. D.: Dynamics of North Patagonian rainforests from fine-resolu-
1256 tion pollen, charcoal and tree-ring analysis, Chonos Archipelago, Southern Chile, *Austral Ecol.*, 28, 413–
1257 422, doi:10.1046/j.1442-9993.2003.01299.x , 2003.
- 1258 Takahashi, K., and Battisti, D.: Processes controlling the mean tropical pacific precipitation pattern. Part I: The Andes
1259 and the eastern Pacific ITCZ. *Journal of Climate*, 20(14), 3434-3451, 2007a.
- 1260 Takahashi, K., and Battisti, D.: Processes controlling the mean tropical pacific precipitation pattern. Part II: The SPCZ

- 1261 and the southeast Pacific dry zone. *Journal of Climate*, 20(23), 5696-5706, 2007b.
- 1262 Tang, L., Shen, S., Liu, K., and Overpeck, J. T.: Changes in South Asian monsoon: new high-resolution pa-
1263 leoclimatic records from Tibet, China, *Chinese Sci. Bull.*, 45, 87-91, doi:10.1007/BF02884911, 2000.
- 1264 Thiede, R.C., and Ehlers, T.A.: Large spatial and temporal variations in Himalayan denudation. *Earth and Planetary*
1265 *Science Letters*, 374, 256-257. doi:10.1016/j.epsl.2013.03.004, 2013.
- 1266 Thomas, A.: The climate of the Gongga Shan range, Sichuan Province, PR China. *Arctic and Alpine Research*, 29(2),
1267 226-232, 1997.
- 1268 Uppala, S.M., Kållberg, P.W., Simmons, A.J., Andrae, U., da Costa Bechtold, V., Fiorino, M., Gibson, J.K., Haseler, J.,
1269 Hernandez, A., Kelly, G.A., Li, X., Onogi, K., Saarinen, S., Sokka, N., Allan, R.P., Andersson, E., Arpe, K.,
1270 Balmaseda, M.A., Beljaars, A.C.M., van de Berg, L., Bidlot, J., Bormann, N., Caires, S., Chevallier, F., Dethof, A.,
1271 Dragosavac, M., Fisher, M., Fuentes, M., Hagemann, S., Hólm, E., Hoskins, B.J., Isaksen, I., Janssen, P.A.E.M.,
1272 Jenne, R., McNally, A.P., Mahfouf, J.-F., Morcrette, J.-J., Rayner, N.A., Saunders, R.W., Simon, P., Sterl, A.,
1273 Trenberth, K.E., Untch, A., Vasiljevic, D., Viterbo, P., and Woollen, J.: The ERA-40 re-analysis. *Quart. J. R.*
1274 *Meteorol. Soc.*, 131, 2961-3012, 2005.
- 1275
- 1276 von Blanckenburg, F., Bouchez, J., Ibarra, D.E., and Maher, K.: Stable runoff and weathering fluxes into the oceans
1277 over Quaternary climate cycles, *Nature Geoscience*, 8(7), 538-542, doi:10.1038/ngeo2452, 2015.
- 1278 Valla, P.G., Shuster, D.L., and van der Beek, P.A.: Significance increase in relief of European Alps during mid-Pleisto-
1279 cene glaciations. *Nature Geoscience*, 4, 688-692. doi:10.1038/ngeo1242, 2011.
- 1280 Van Campo, E., Cour, P., and Huang, S.: Holocene environmental changes in Bangong Co basin (Western
1281 Tibet). Part 2: The pollen record, *Palaeogeogr. Palaeoclimatol.*, 120, 49-63, doi:10.1016/0031-0182(95)00033-
1282 X, 1996.
- 1283
- 1284 Villagrán, C. and Varela, J.: Palynological Evidence for Increased Aridity on the Central Chilean Coast during
1285 the Holocene, *Quaternary Res.*, 34, 198-207, doi:10.1016/0033-5894(90)90031-F, 1990.
- 1286 Villa-Martínez, R., Villagrán, C., and Jenny, B.: The last 7500 cal yr B.P. of westerly rainfall in Central Chile
1287 inferred from a high-resolution pollen record from Laguna Aculeo (34°S), *Quaternary Res.*, 60, 284-293,
1288 doi:https://doi.org/10.1016/j.yqres.2003.07.007, 2003.
- 1289 Wei, W., and Lohmann, G.: Simulated Atlantic Multidecadal Oscillation during the Holocene. *Journal of Climate*, 25,
1290 6989-7002. doi: http://dx.doi.org/10.1175/JCLI-D-11-00667.1, 2012.
- 1291 Wang, R.L., Scarpitta, S. C., Zhang, S. C., and Zheng, M. P.: Later Pleistocene/Holocene climate conditions
1292 of Qinghai-Xizhang Plateau (Tibet) based on carbon and oxygen stable isotopes of Zabuye Lake sedi-
1293 ments, *Earth Planet. Sc. Lett.*, 203, 461-477, doi:10.1016/S0012-821X(02)00829-4, 2002.
- 1294 Whipple, K.X., Kirby, E., and Broecker, S.H.: Geomorphic limits to climate-induced increases in topographic re-
1295 lief. *Nature*, 401, 39-43. doi:10.1038/43375, 1999.
- 1296 Whipple, K.X., and Tucker, G.E.: Dynamics of the stream-power river incision model: Implications for height limits of

- 1297 mountain ranges, landscape response timescales, and research needs, *Journal of Geophysical Research-Solid Earth*,
1298 104, 17661-17674, 1999.
- 1299 Whipple, K. X.: The influence of climate on the tectonic evolution of mountain belts, *Nat. Geosci.*, 2, doi:10.1038/
1300 ngeo413, 2009.
- 1301 Wilks, D.S.: Statistical methods in the atmospheric sciences - 3rd ed. Academic Press, Oxford, 2011.
- 1302 Willett, S.D., Schlunegger, F., and Picotti, V.: Messinian climate change and erosional destruction of the central
1303 European Alps. *Geology*, 34(8), 613-616, 2006.
- 1304 Wilson, G.S., Barron, J.A., Ashworth, A.C., Askin, R.A., Carter, J.A., Curren, M.G., Dalhuisen, D.H., Friedmann, E.I.,
1305 Fyodorov-Davidov, D.G., Gilichinsky, D.A., Harper, M.A., Harwood, D.M., Hiemstra, J.F., Janecek, T.R., Licht,
1306 K.J., Ostroumov, V.E., Powell, R.D., Rivkina, E.M., Rose, S.A., Stroeven, A.P., Stroeven, P., van der Meer, J.J.M.,
1307 Wizevich, M.C.: The Mount Feather Diamicton of the Sirius Group: an accumulation of indicators of Neogene Ant-
1308 arctic glacial and climatic history, *Palaeogeography, Palaeoclimatology, Palaeoecology*, 182 (1–2), 117–131, 2002.
- 1309 Wischniewski, J., Mischke, S., Wang, Y., and Herzsuh, U.: Reconstructing climate variability on the
1310 northeastern Tibetan Plateau since the last lateglacial – a multi-proxy, dual-site approach comparing
1311 terrestrial and aquatic signals, *Quaternary Science Reviews*, 30, 82-97,
1312 doi:10.1016/j.quascirev.2010.10.001, 2011.
- 1313 Wünnemann, B., Mischke, S., and Chen, F.: A Holocene sedimentary record from Bosten lake, China, *Pa-
1314 laeogeogr. Palaeocl.*, 234, 223-238, doi:10.1016/j.palaeo.2005.10.016, 2006.
- 1315 Yanhong, W., Lücke, A., Zhangdong, J., Sumin, W., Schleser, G.H., Battarbee, R.W., and Weilan, X.: Holo-
1316 cene climate development on the central Tibetan Plateau: A sedimentary record from Cuoe Lake, *Palaeo-
1317 geogr. Palaeocl.*, 234, 328-340, doi:10.1016/j.palaeo.2005.09.017, 2006
- 1318 Yanites, B.J., and Ehlers, T.A.: Global climate and tectonic controls on the denudation of glaciated mountains. *Earth
1319 and Planetary Science Letters*, 325, 63-75, 2012.
- 1320 Yu, L. and Lai, Z.: Holocene climate change inferred from stratigraphy and OSL chronology of Aeolian sedi-
1321 ments in the Qaidam Basin, northeastern Qinghai-Tibetan Plateau, *Quaternary Res.*, 81, 488-499,
1322 doi:10.1016/j.yqres.2013.09.006, 2014.
- 1323 Zhang, C. and Mischke, S.: A lateglacial and Holocene lake record from the Nianbaoyeze Mountains and in-
1324 ferences of lake, glacier and climate evolution on the eastern Tibetan Plateau, *Quaternary Sci. Rev.*, 28,
1325 1970-1983, doi:10.1016/j.quascirev.2009.03.007, 2009.
- 1326 Zhang, J., Chen, F., Holmes, J. A., Li, H., Guao, X., Wang, J., Li, S., Lu, Y., Zhao, Y., and Qiang, M.: Holo-
1327 cene monsoon climate documented by oxygen and carbon isotopes from lake sediments and peat bogs
1328 in China: a review and synthesis, *Quaternary Sci. Rev.*, 30, 1973-1987, doi:10.1016/
1329 j.quascirev.2011.04.023, 2011.
- 1330 Zhang, X., Lohmann, G., Knorr, G., and Xu X.: Different ocean states and transient characteristics in Last Glacial Max-
1331 imum simulations and implications for deglaciation. *Clim. Past*, 9, 2319-2333, doi:10.5194/cp-9-2319-2013, 2013a.

1332 Zhang, R., Yan, Q., Zhang, Z.S., Jiang, D., Otto-Bliesner, B.L., Haywood, A.M., Hill, D.J., Dolan, A.M., Stepanek, C.,
1333 Lohmann, G., Contoux, C., Bragg, F., Chan, W.-L., Chandler, M.A., Jost, A., Kamae, Y., Abe-Ouchi, A., Ramstein,
1334 G., Rosenbloom, N.A., Sohl, L., and Ueda, H.: East Asian monsoon climate simulated in the PlioMIP. *Clim. Past*, 9,
1335 2085-2099, doi:10.5194/cp-9-2085-2013, 2013b.

1336

1337 Zhang, X., Lohmann, G., Knorr, G., and Purcell C.: Abrupt glacial climate shifts controlled by ice sheet changes.
1338 *Nature*, 512 (7514), 290-294, doi:10.1038/nature13592, 2014.

1339 Zhisheng, A., Kutzbach, J.E., Prell, W.L., and Porter, S.C.: Evolution of Asian monsoons and phased uplift of the South
1340 Asian plateau since Late Miocene times. *Nature*, 411(6833), 62-66, 2001.

1341 Zhou, W. J., Lu, X. F., Wu, Z. K., Deng, L., Jull, A. J. T., Donahue, D. J., and Beck, W.: Peat record reflecting
1342 Holocene climate change in the Zoigê Plateau and AMS radiocarbon dating, *Chinese Sci. Bull.*, 47, 66-
1343 70, doi:10.1360/02tb9013, 2002.

1344
1345
1346
1347
1348
1349
1350
1351
1352
1353
1354
1355
1356
1357
1358
1359
1360
1361
1362
1363
1364
1365
1366
1367
1368
1369
1370
1371
1372
1373
1374
1375
1376
1377
1378
1379
1380
1381

1382
1383
1384
1385
1386
1387
1388
1389
1390
1391
1392
1393
1394
1395
1396
1397
1398
1399
1400
1401
1402
1403
1404
1405
1406
1407
1408
1409
1410
1411
1412
1413
1414
1415
1416
1417
1418
1419
1420
1421
1422
1423
1424
1425
1426
1427
1428
1429
1430
1431
1432
1433
1434
1435
1436
1437
1438
1439
1440

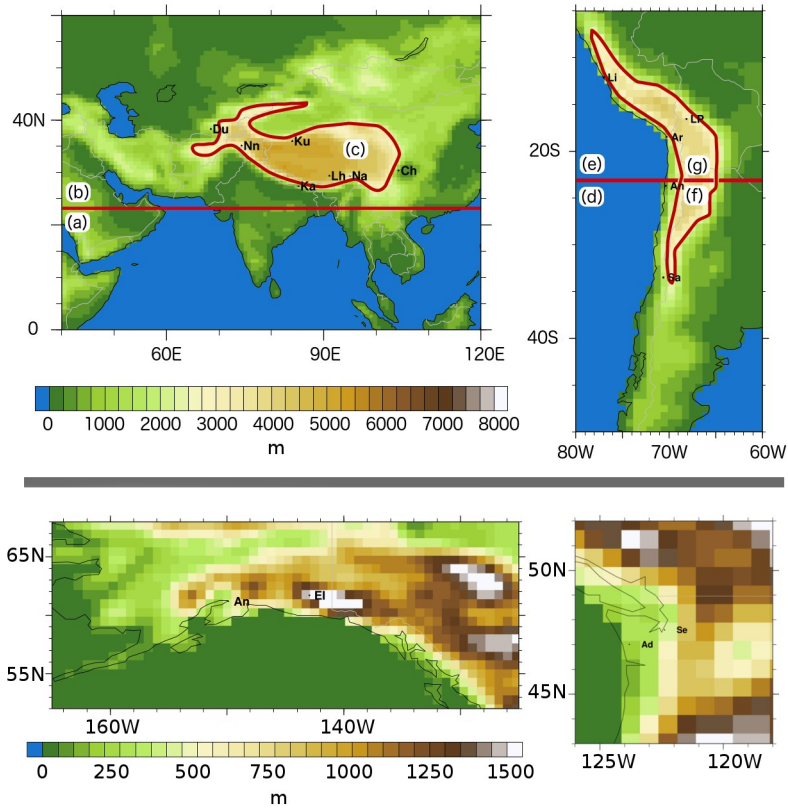


Figure 1

1441
1442
1443
1444
1445
1446
1447
1448
1449
1450
1451
1452
1453
1454
1455
1456
1457
1458
1459
1460
1461
1462
1463
1464
1465
1466
1467
1468
1469
1470
1471
1472
1473
1474
1475
1476
1477
1478
1479
1480
1481
1482
1483
1484
1485
1486
1487
1488
1489
1490
1491
1492
1493
1494
1495
1496
1497
1498
1499
1500

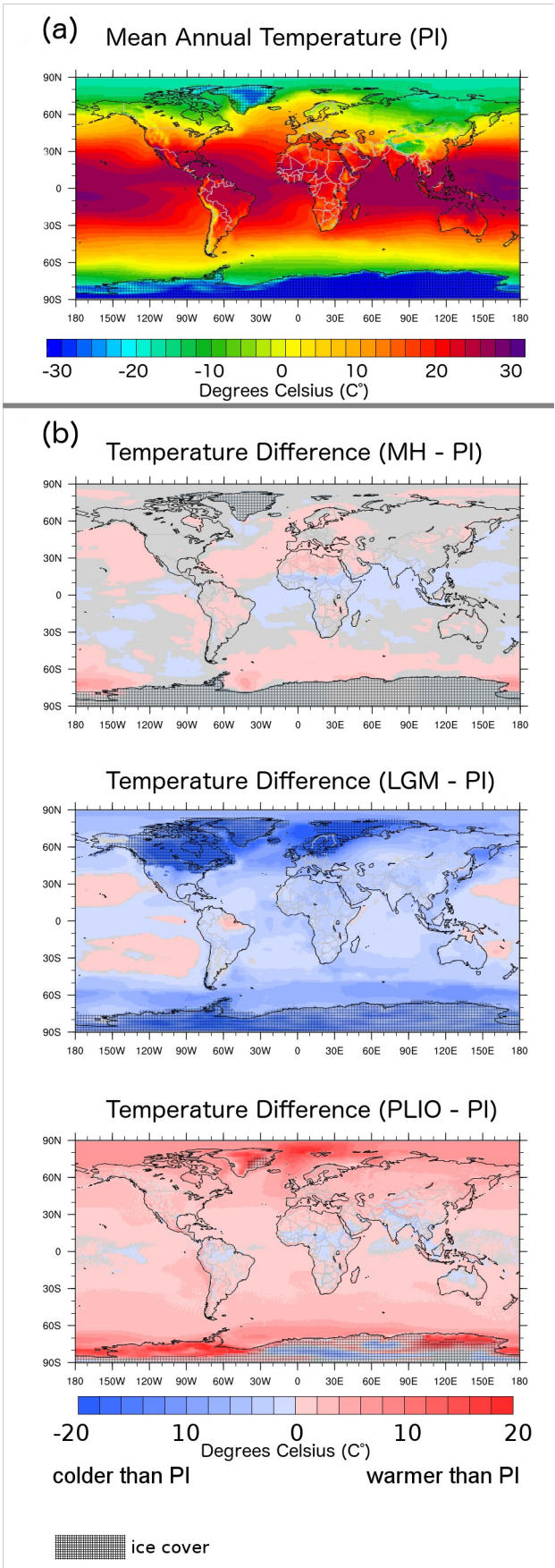


Figure 2

1501
1502
1503
1504
1505
1506
1507
1508
1509
1510
1511
1512
1513
1514
1515
1516
1517
1518
1519
1520
1521
1522
1523
1524
1525
1526
1527
1528
1529
1530
1531
1532
1533
1534
1535
1536
1537
1538
1539
1540
1541
1542
1543
1544
1545
1546
1547
1548
1549
1550
1551
1552
1553
1554
1555
1556
1557
1558
1559
1560

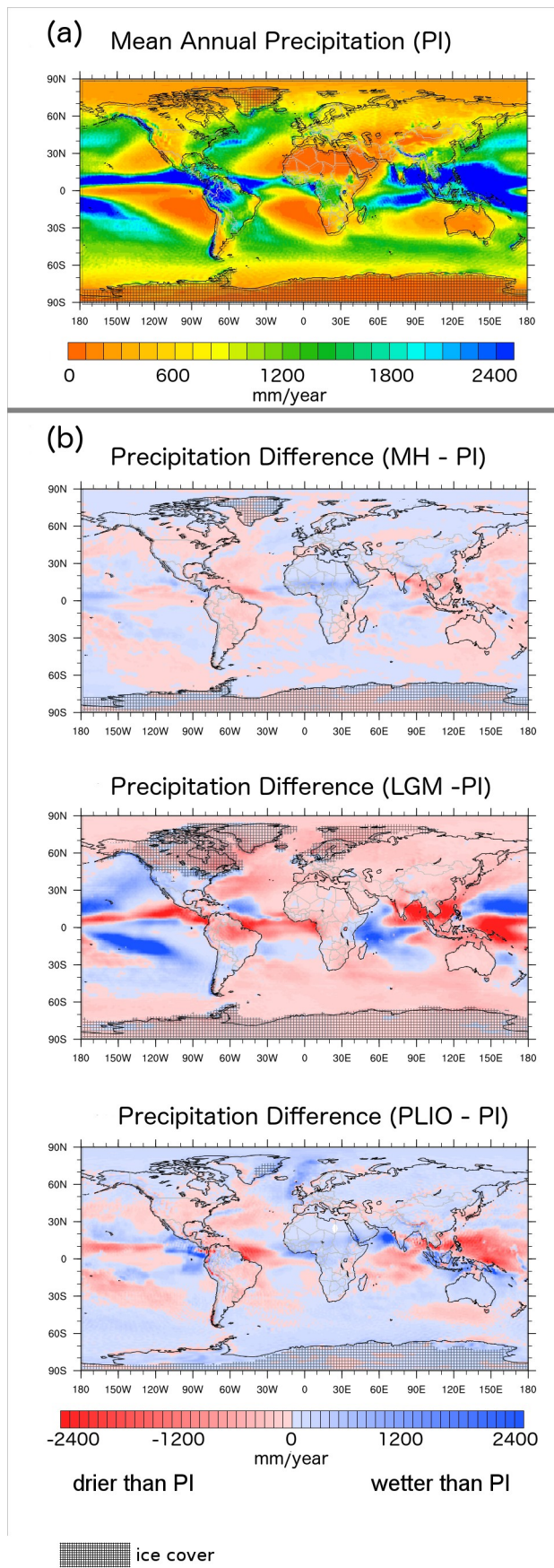


Figure 3

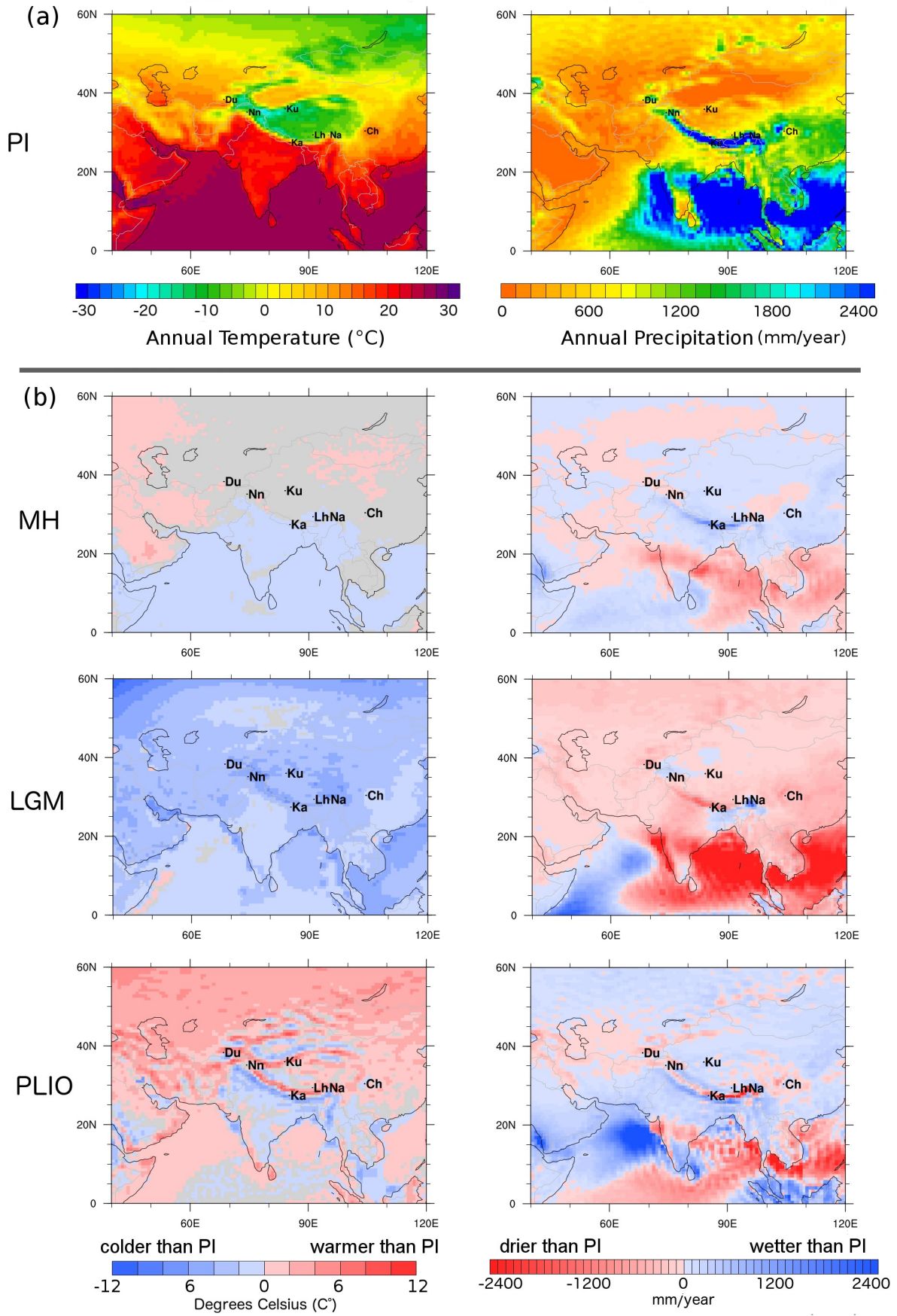


Figure 4

1564
1565
1566
1567
1568
1569
1570
1571
1572
1573
1574
1575
1576
1577
1578
1579
1580
1581
1582
1583
1584
1585
1586
1587
1588
1589
1590
1591
1592
1593
1594
1595
1596
1597
1598
1599
1600
1601
1602
1603
1604
1605
1606
1607
1608
1609
1610
1611
1612
1613
1614
1615
1616
1617
1618
1619
1620
1621
1622
1623

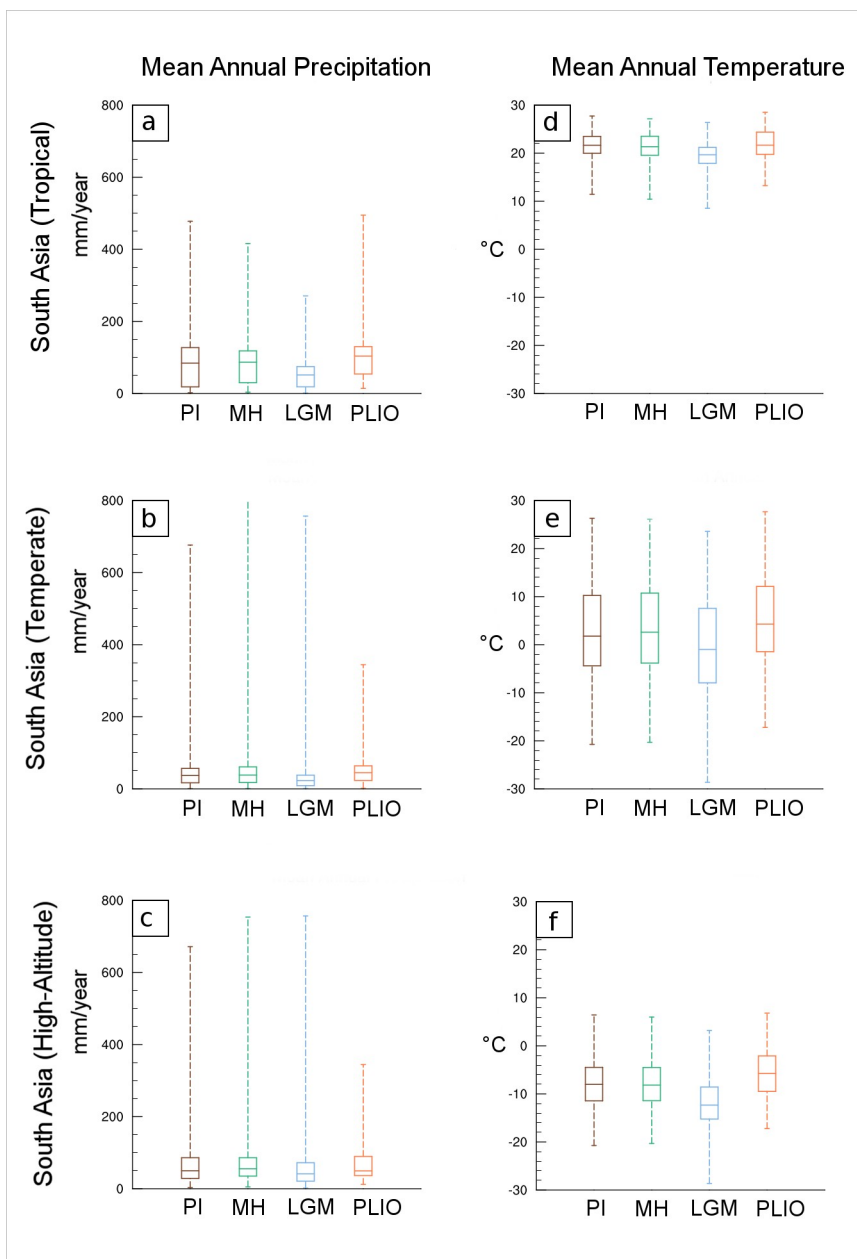


Figure 5

1624
1625
1626
1627
1628
1629
1630
1631
1632
1633
1634
1635
1636
1637
1638
1639
1640
1641
1642
1643
1644
1645
1646
1647
1648
1649
1650
1651
1652
1653
1654
1655
1656
1657
1658
1659
1660
1661
1662
1663
1664
1665
1666
1667
1668
1669
1670
1671
1672
1673
1674
1675
1676
1677
1678
1679
1680
1681
1682
1683

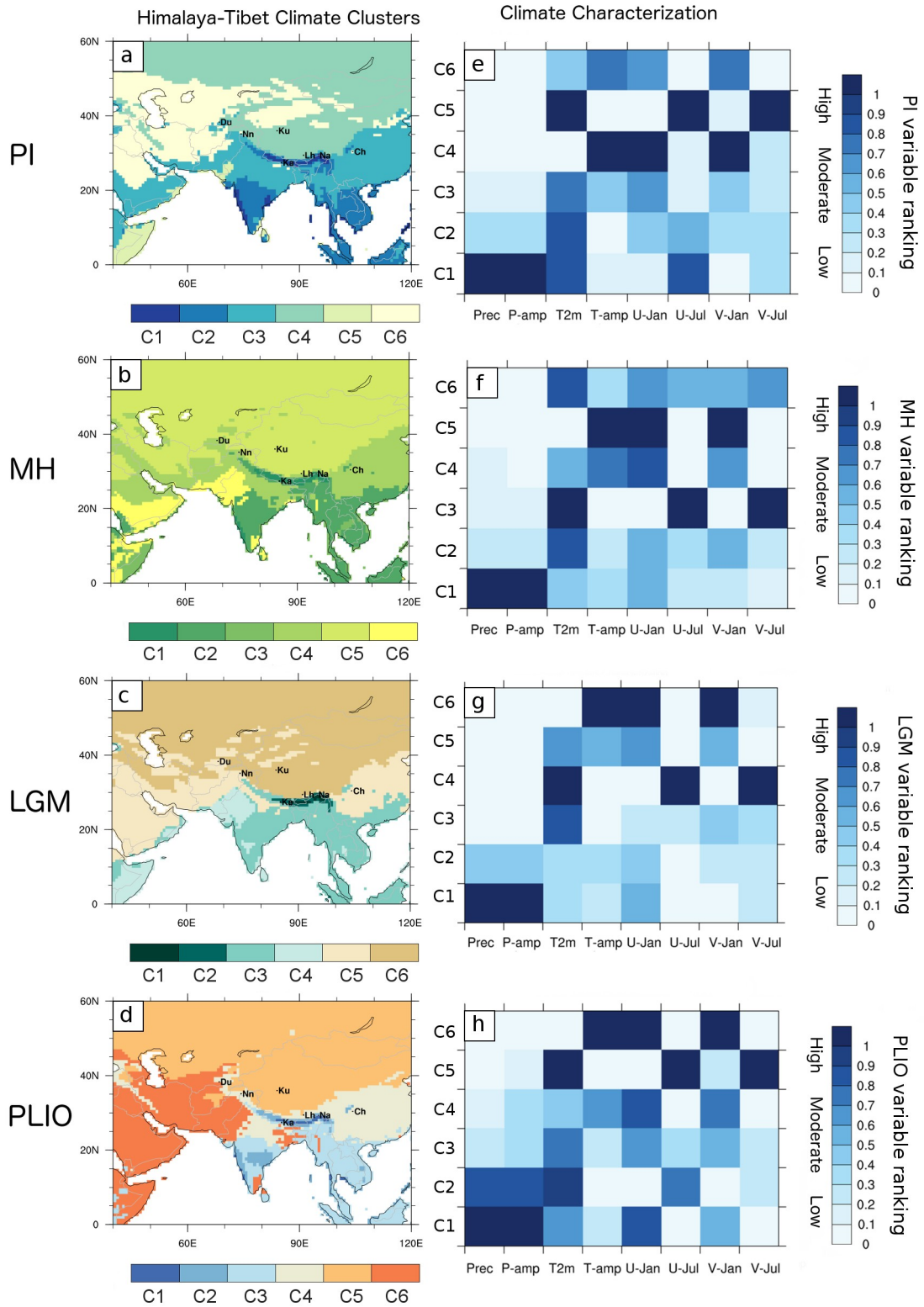


Figure 6

1684
 1685
 1686
 1687
 1688
 1689
 1690
 1691
 1692
 1693
 1694
 1695
 1696
 1697
 1698
 1699
 1700
 1701
 1702
 1703
 1704
 1705
 1706
 1707
 1708
 1709
 1710
 1711
 1712
 1713
 1714
 1715
 1716
 1717
 1718
 1719
 1720
 1721
 1722
 1723
 1724
 1725
 1726
 1727
 1728
 1729
 1730
 1731
 1732
 1733
 1734
 1735
 1736
 1737
 1738
 1739
 1740
 1741
 1742
 1743

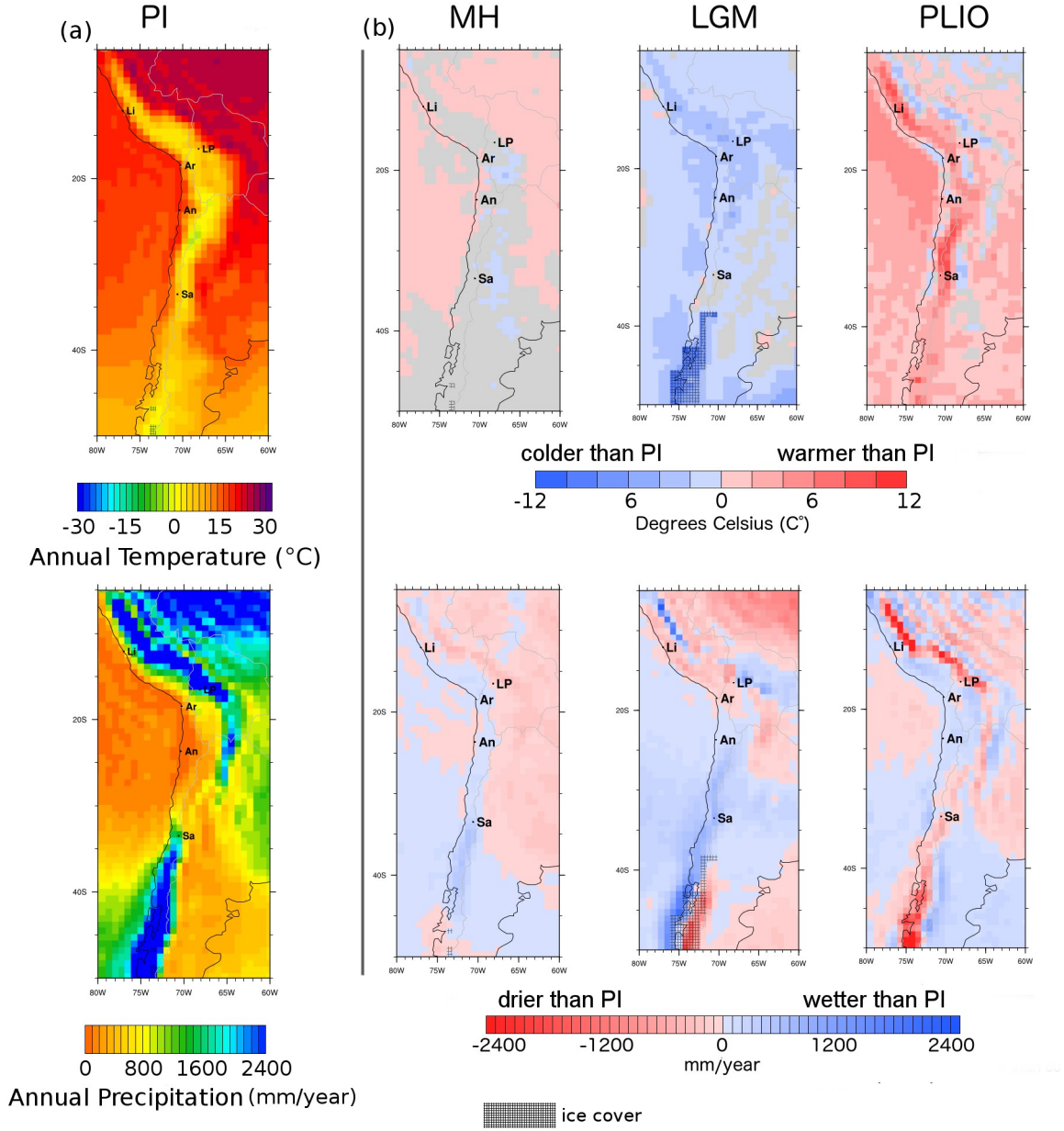


Figure 7

1744
1745
1746
1747
1748
1749
1750
1751
1752
1753
1754
1755
1756
1757
1758
1759
1760
1761
1762
1763
1764
1765
1766
1767
1768
1769
1770
1771
1772
1773
1774
1775
1776
1777
1778
1779
1780
1781
1782
1783
1784
1785
1786
1787
1788
1789
1790
1791
1792
1793
1794
1795
1796
1797
1798
1799
1800
1801
1802
1803

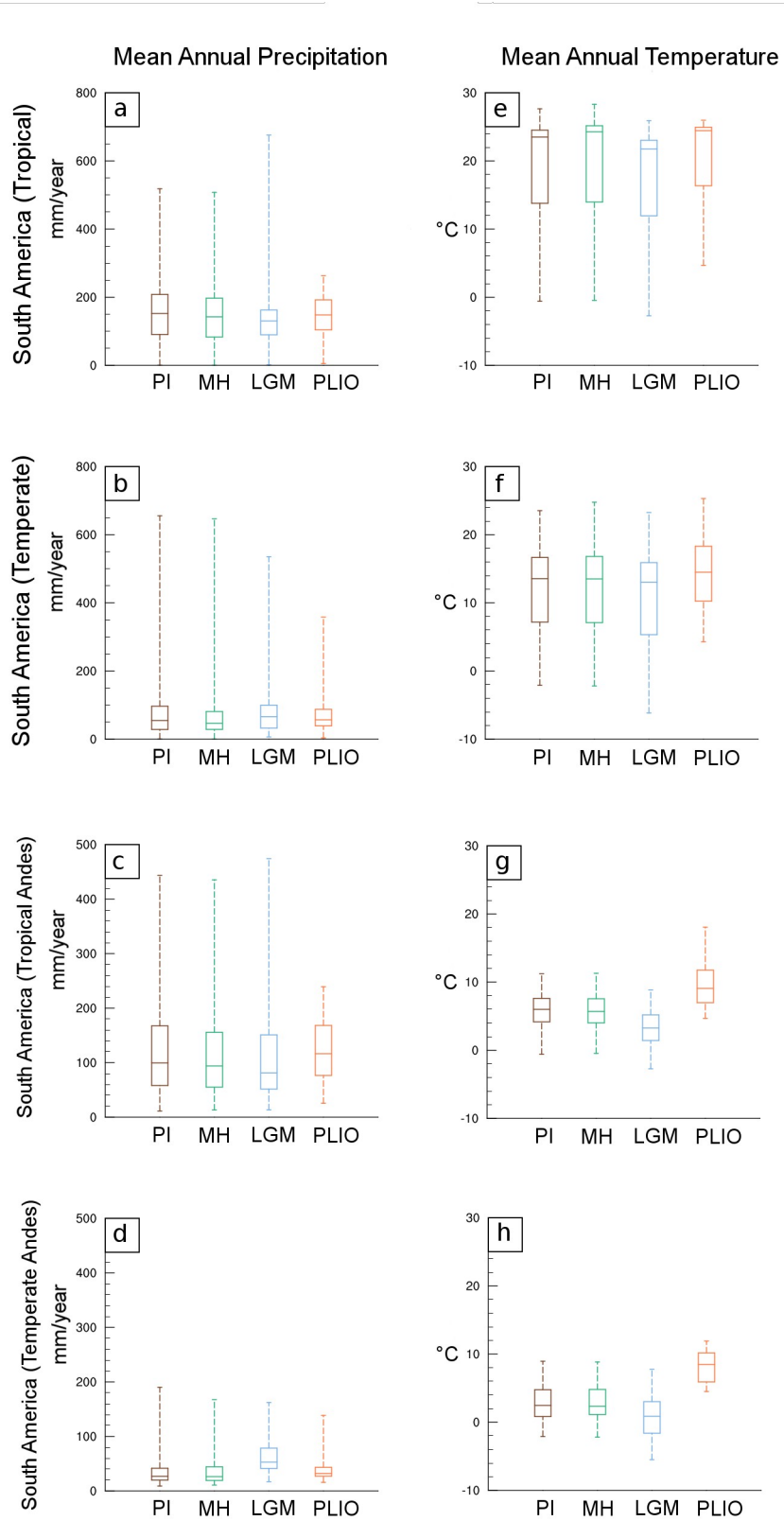


Figure 8

1804
 1805
 1806
 1807
 1808
 1809
 1810
 1811
 1812
 1813
 1814
 1815
 1816
 1817
 1818
 1819
 1820
 1821
 1822
 1823
 1824
 1825
 1826
 1827
 1828
 1829
 1830
 1831
 1832
 1833
 1834
 1835
 1836
 1837
 1838
 1839
 1840
 1841
 1842
 1843
 1844
 1845
 1846
 1847
 1848
 1849
 1850
 1851
 1852
 1853
 1854
 1855
 1856
 1857
 1858
 1859
 1860
 1861
 1862
 1863

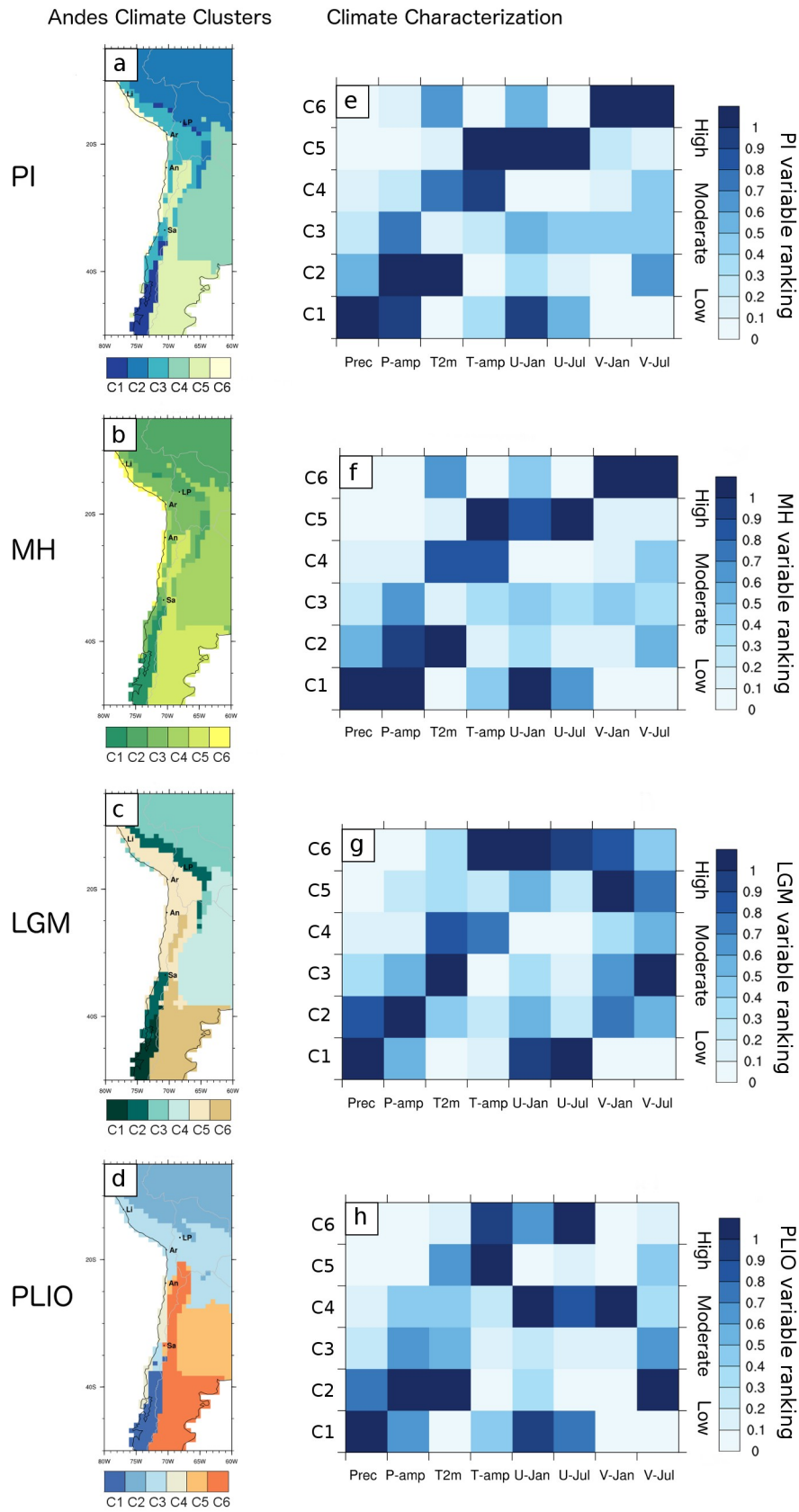


Figure 9

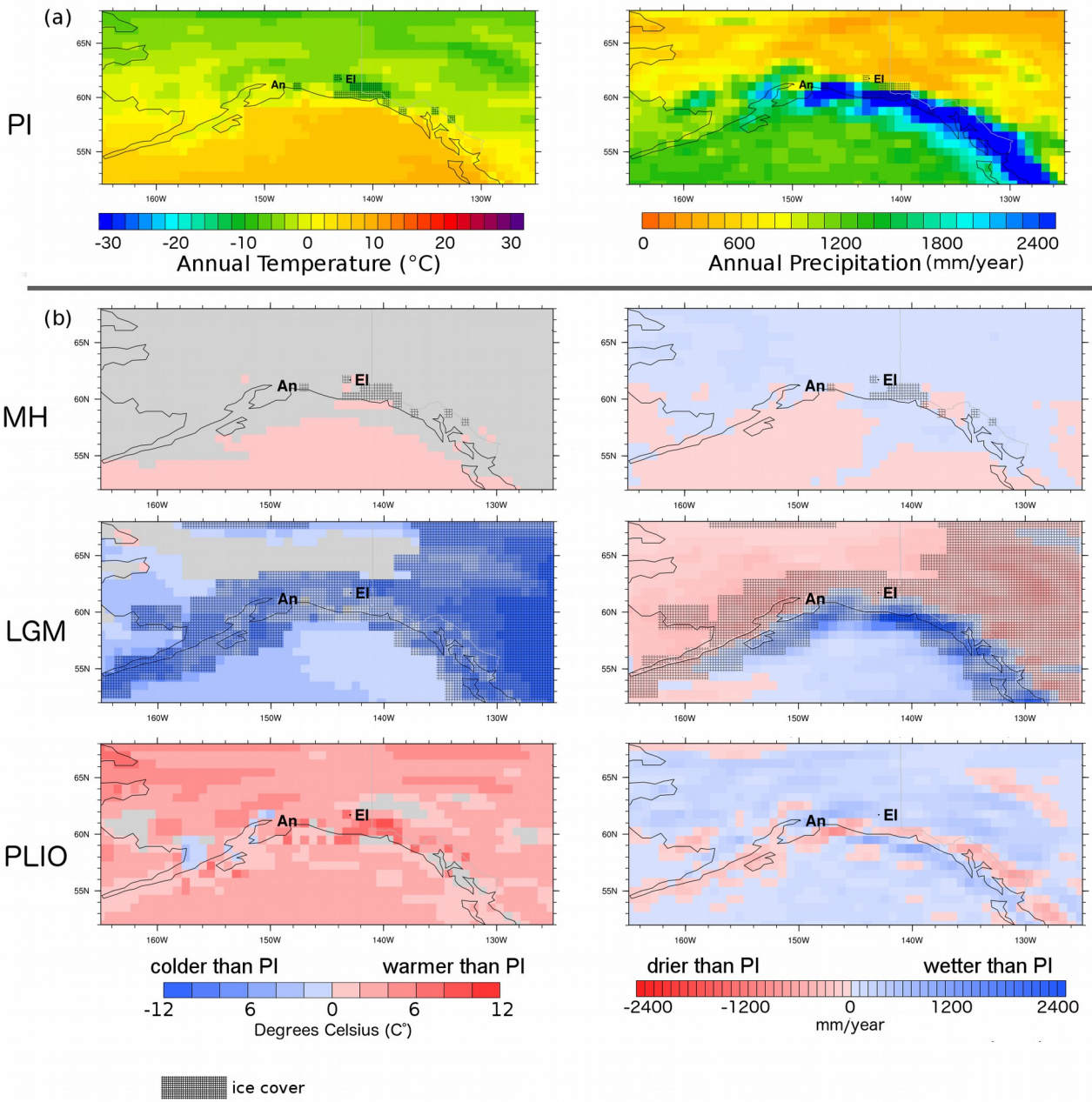


Figure 10

1865
1866
1867
1868
1869
1870
1871
1872
1873
1874
1875
1876
1877
1878
1879
1880
1881
1882

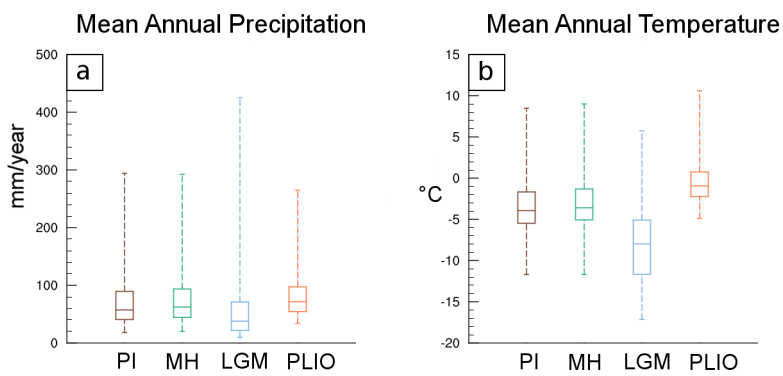


Figure 11

1883
 1884
 1885
 1886
 1887
 1888
 1889
 1890
 1891
 1892
 1893
 1894
 1895
 1896
 1897
 1898
 1899
 1900
 1901
 1902
 1903
 1904
 1905
 1906
 1907
 1908
 1909
 1910
 1911
 1912
 1913
 1914
 1915
 1916
 1917
 1918
 1919
 1920
 1921
 1922
 1923
 1924
 1925
 1926
 1927
 1928
 1929
 1930
 1931
 1932
 1933
 1934
 1935
 1936
 1937
 1938
 1939
 1940
 1941
 1942

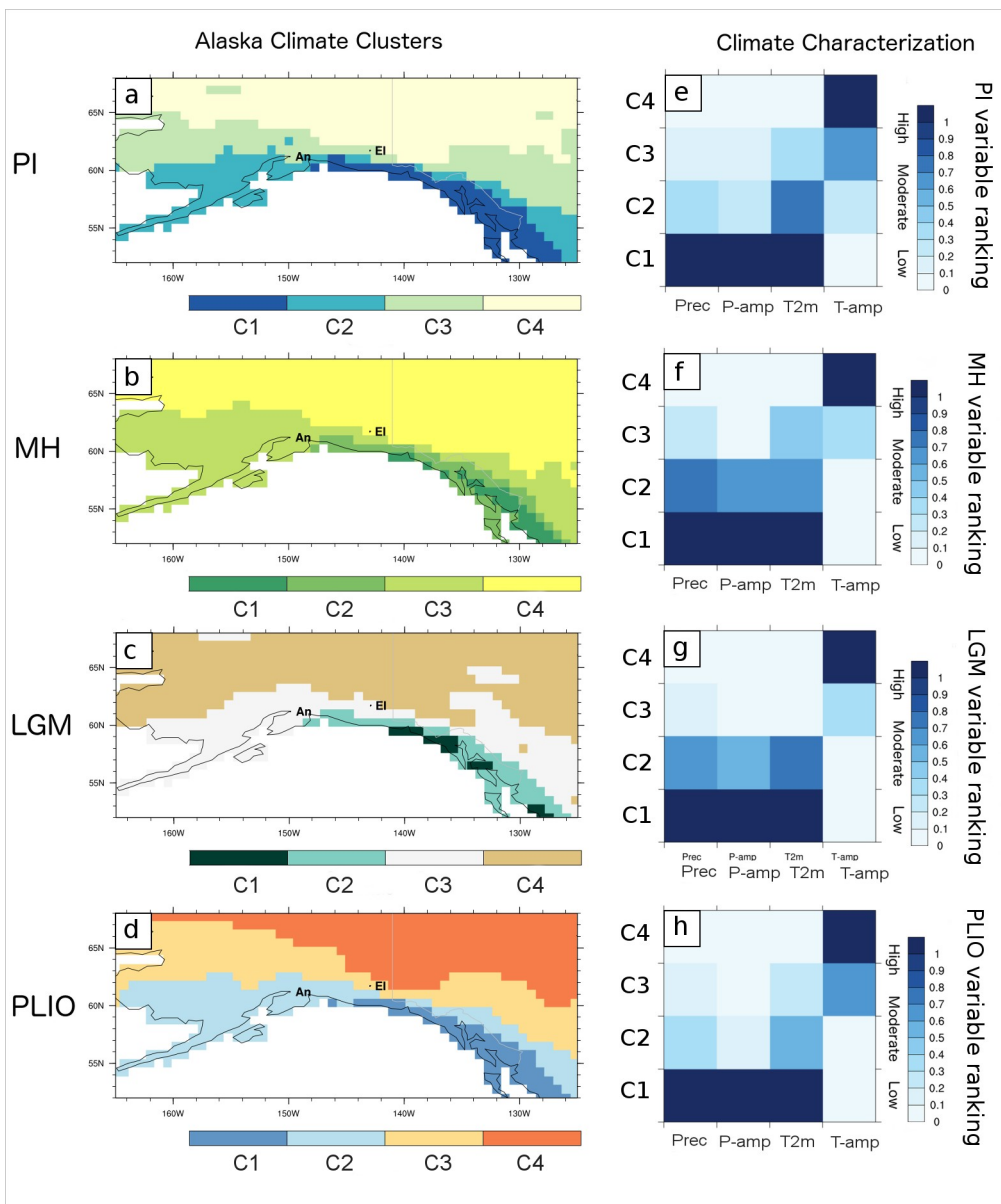


Figure 12

1943
1944
1945
1946
1947
1948
1949
1950
1951
1952
1953
1954
1955
1956
1957
1958
1959
1960
1961
1962
1963
1964
1965
1966
1967
1968
1969
1970
1971
1972
1973
1974
1975
1976
1977
1978
1979
1980
1981
1982
1983
1984
1985
1986
1987
1988
1989
1990
1991
1992
1993
1994
1995
1996
1997
1998
1999
2000
2001
2002

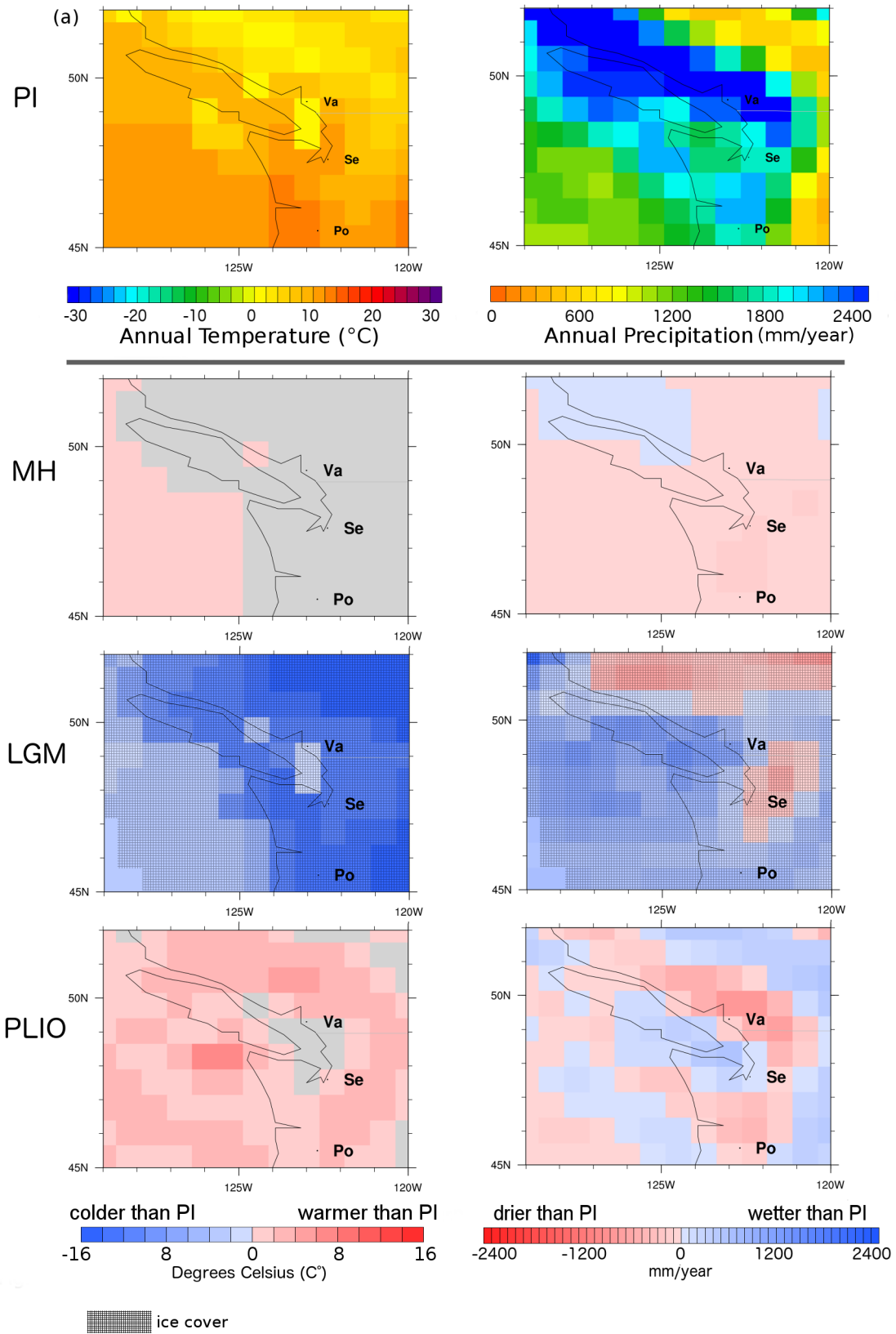


Figure 13

2003
 2004
 2005
 2006
 2007
 2008
 2009
 2010
 2011
 2012
 2013
 2014
 2015
 2016
 2017
 2018
 2019
 2020
 2021
 2022
 2023
 2024
 2025
 2026
 2027
 2028
 2029
 2030
 2031
 2032
 2033
 2034
 2035
 2036
 2037
 2038
 2039
 2040
 2041
 2042
 2043
 2044
 2045
 2046
 2047
 2048
 2049
 2050
 2051
 2052
 2053
 2054
 2055
 2056
 2057
 2058
 2059
 2060
 2061
 2062

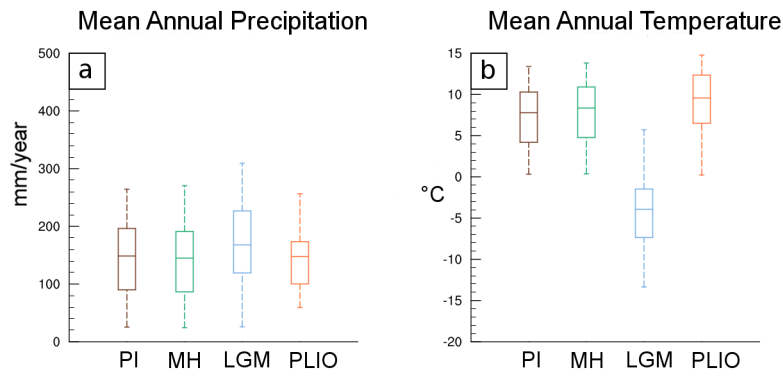


Figure 14

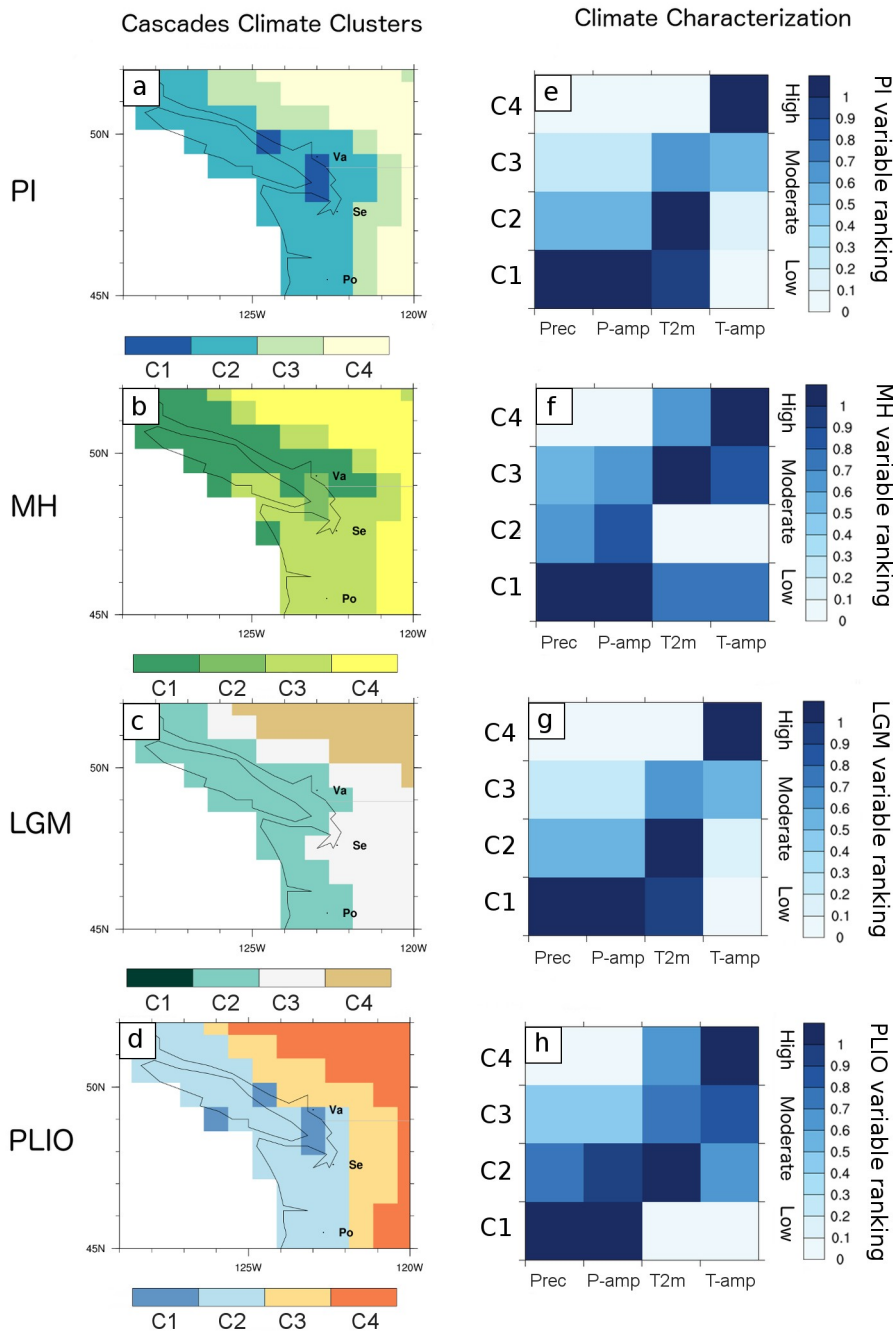


Figure 15

2063
2064
2065
2066
2067
2068
2069
2070

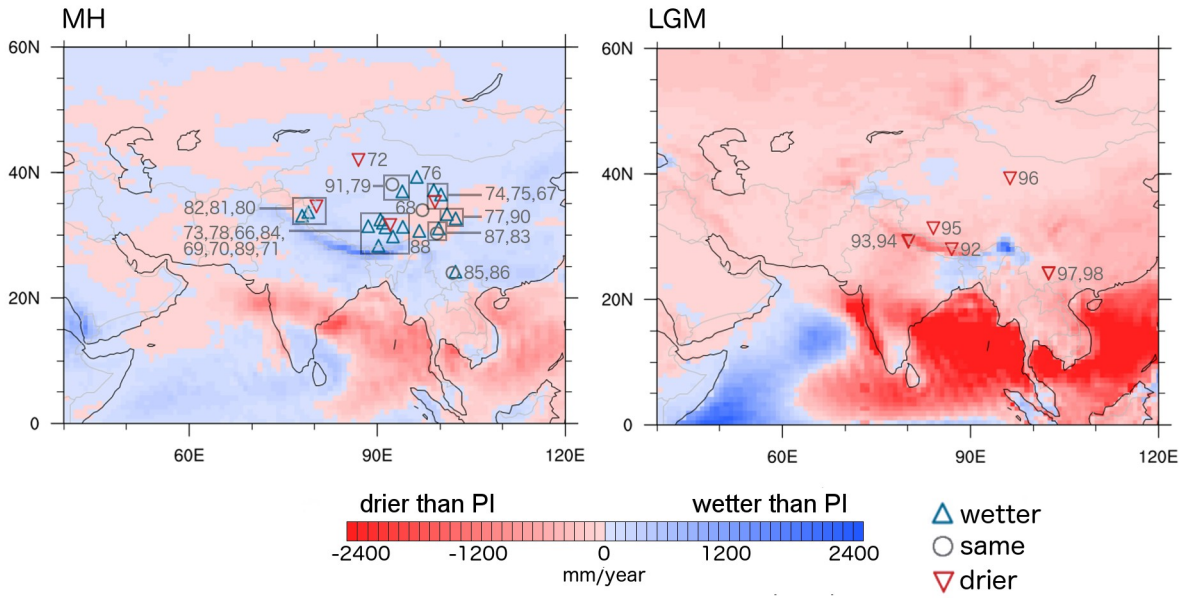


Figure 16

2071
2072
2073
2074
2075
2076
2077
2078
2079
2080
2081
2082
2083
2084
2085
2086
2087
2088
2089
2090
2091
2092
2093
2094
2095
2096
2097
2098
2099
2100

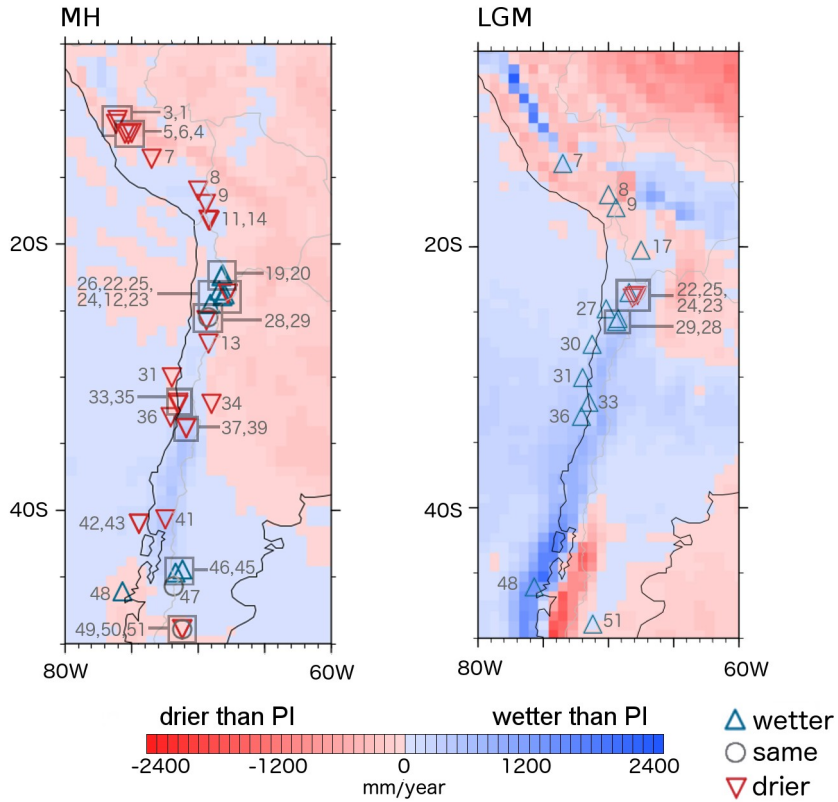


Figure 17